Ore Geology Reviews 159 (2023) 105580

Contents lists available at ScienceDirect

Ore Geology Reviews

journal homepage: www.elsevier.com/locate/oregeorev

Ore-forming process of the Huize super-large Pb-Zn deposit, SW China: Constraints from in situ elements and S-Pb isotopes

Mao Tan [a,b], Xiao-Wen Huang [a,*], Peng Wu [c], Zhilong Huang [a,*]

[a] State Key Laboratory of Ore Deposit Geochemistry, Institute of Geochemistry, Chinese Academy of Sciences, Guiyang 550081, China
[b] University of Chinese Academy of Sciences, Beijing 100049, China
[c] Faculty of Land Resources Engineering, Kunming University of Science and Technology, Kunming 650093, China

ARTICLE INFO

Keywords:
Ore-forming process
Fluid evolution
In situ trace element and isotopes
Huize Pb-Zn deposit

ABSTRACT

Study on the ore-forming process is crucial for comprehending the mechanisms of metal enrichment and facilitating mineral exploration. The Huize deposit in southwestern China is characterized by significant Pb and Zn resources, as well as economic coproducts of Ge and Ag. In spite of extensive studies, the key factors for ore deposition remain controversial. Mineral textures, in situ trace elements of dolomite, and S and Pb isotopes of sphalerite and galena from the contact zone between ore body and wall rocks were used to decipher this issue. The contact zone samples are further divided into three parts at the thin section scale: ore, transitional zone, and wall rock dolostone. In the ore part, dolomite is characterized by irregular replacement. In the transitional zone, dolomite displays a core-rim texture with dolomite in the core and Fe- and Mn-rich dolomite in the rim. In the wall rock part, the Fe- and Mn-rich dolomite occur as veins. From the ore, through the transitional zone, to the wall rock, the contents of Ca, Mg, and rare earth elements in dolomite increased, whereas the contents of Mn, Fe, In, and V decreased, indicating interaction between ore-forming fluids and dolostone. The LREE depletion of hydrothermal dolomite in three zones is caused by fluid-rock interaction and retention of Cl^- complexes. Negative Eu and Ce anomalies indicate that fluids evolve from alkaline to weakly acidic at relatively low temperatures. The $\delta^{34}S$ values of sphalerite generally decrease from the ore to the transitional zone, consistent with the kinetic fractionation of sulfur isotopes due to the precipitation of sulfides. The Pb isotopic composition of galena generally increases from the ore, transitional zone, to the wall rock, reflecting increased involvement of dolostone. The detailed ore-forming process can be summarized as follows. When hydrothermal fluids, with higher ore elements, higher $\delta^{34}S$ value, and low Pb isotope composition, enter the wall rock that has relatively high Pb isotopic composition, intense fluid-rock interaction occurs, and elements and isotopes are exchanged, forming dolomite-dominated alteration and Pb-Zn sulfides. During this process, the fluids evolve from alkaline to neutral and weakly acidic. Therefore, we suggest that the change in the pH due to the replacement of dolostone has played an important role in ore deposition.

1. Introduction

The Sichuan-Yunnan-Guizhou (SYG) Pb-Zn metallogenic province is located on the southwestern margin of the Yangtze Block, with a complex geological environment and superior metallogenic conditions (Han et al., 2014). The SYG district is an important component of the low-temperature metallogenic domain of South China (Hu et al., 2017). The SYG district contains more than 400 Pb-Zn deposits and occurrences, which is the main source of Pb and Zn in China (Liu and Lin, 1999; Huang et al., 2004; Hu and Zhou, 2012; Zhou et al., 2013d; Ye et al., 2012, 2016; Hu et al., 2017; Tan et al., 2017; Wang et al., 2018; Luo et al., 2019a, b). The Huize deposit is a super-large Pb-Zn deposit in the SYG district, with exceptionally high Pb and Zn grade (25–35% Pb and Zn), and high contents of Ge, Cd, In, and Ag in the ores (Ye et al., 2011).

The Huize Pb-Zn deposit has been widely studied in many aspects, including geological features (Liu and Lin, 1999; Han et al., 2004; Han et al., 2007), the source of the ore-forming fluids (Zhou et al., 2001; Li et al., 2006; Li et al., 2007a, Li et al., 2007b; Xu et al., 2020; Oyebamiji et al., 2020a, Zhu et al., 2021), the age of mineralization (Li et al., 2007b; Huang et al., 2010; Tang et al., 2019), and classification for deposit types (Zhang et al., 2017; Meng et al., 2019). Different models

* Corresponding authors.
E-mail addresses: huangxiaowen@mail.gyig.ac.cn (X.-W. Huang), huangzhilong@vip.gyig.ac.cn (Z. Huang).

https://doi.org/10.1016/j.oregeorev.2023.105580
Received 15 February 2023; Received in revised form 6 July 2023; Accepted 21 July 2023
Available online 22 July 2023

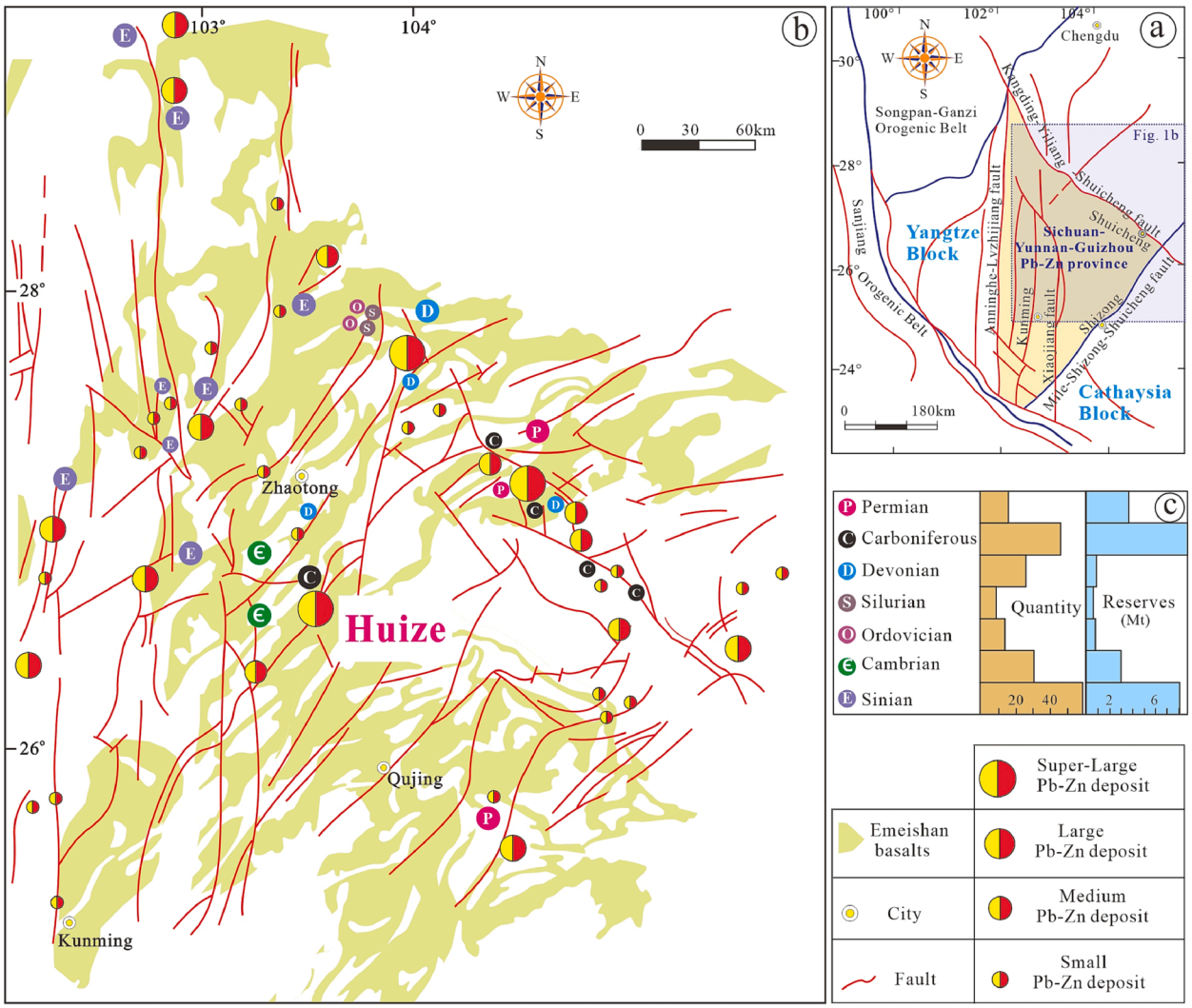

Fig. 1. (a) The location of Sichuan-Yunnan-Guizhou Pb-Zn metallogenic province in the Yangtze Block; (b) Distribution of Pb-Zn deposits in the SYG metallogenic province with emphasis of the location of Huize deposit; (c) Ore-hosting wall rocks and deposit scale of Pb-Zn deposits in Sichuan-Yunnan-Guizhou region (modified after Ye et al., 2011; Zhou et al., 2018b).

have been proposed to explain the ore-forming process at the Huize deposit. Bao et al. (2017) suggested that the secular interaction between the deep-circulating fluids and the clastic sequence of the Kunyang Group is possibly the major reason for sulfide precipitation. The carbonate-ore fluids interaction causes the fluid pH changing from acidic to neutral, instability of Pb and Zn chloride complexes, hydrolysis of Pb and Zn ions, and subsequent precipitation of sulfides (Zhang et al., 2019). Zhang et al. (2022) indicated that the deep fluids with medium–high temperature, low salinity and acidity, metal-rich and lighter C and O isotopes mixed with shallow fluids enriched with H_2S, with low temperature, high salinity, weak alkalinity, lighter S isotopes, heavier C–O and H–O isotopes under reduced pressure, leading to the precipitation of galena and sphalerite. The evaporated brines entered and disseminated in metal-fertile sedimentary/basement sequences along fractures and interlayer fracture zones, resulting in intense fluid-rock interaction and effective leaching of metals such as Pb and Zn (Oyebamiji et al., 2023). These studies provide constraints on the ore-forming process of the Huize Pb–Zn deposits at a macro scale (e.g. deposit scale). However, the study of the ore-forming process from the micro scale is relatively rare.

Previous studies summarized the dolostone characteristics from mineralization-alteration zoning in the Huize Pb-Zn deposit (Wen et al., 2014; Li et al., 2017). These studies indicated that the sequential arrangement of rock types from ore body to wall rock is as follows: Pb-Zn ore → mineralized coarse-grained dolostone → gray coarse-grained dolostone → beige coarse-grained dolostone. With decreasing distance from the ore body, the content of CaO and MgO in dolomite decrease gradually, but the contents of TFe and MnO increase. The systematic variations in textures of dolostone and the composition of dolomite from the alteration zone to the ore body indicated that dolomite can serve as a reliable indicator for the ore-forming process in Pb-Zn deposits.

In this study, in situ trace element composition of dolomite, S and Pb isotopic composition of sphalerite and galena in the ore, transitional zone, and wall rock dolostone of the Huize deposit were analyzed to identify changes in composition and isotopic during alteration and mineralization. The new data were used to constrain the systematic variations in composition of hydrothermal fluids and physiochemical conditions. This study will provide new constraints on detailed ore-forming process of the Huize Pb-Zn deposit.

2. Regional geology

The SYG metallogenic province is located at the southwestern margin of the Yangtze Block (Fig. 1a) and contains more than 400 Pb-Zn deposits. These deposits are spread within the “triangle” (Fig. 1b) bounded by the north–south Xiaojiang fault, the north-east Mile-Shizong

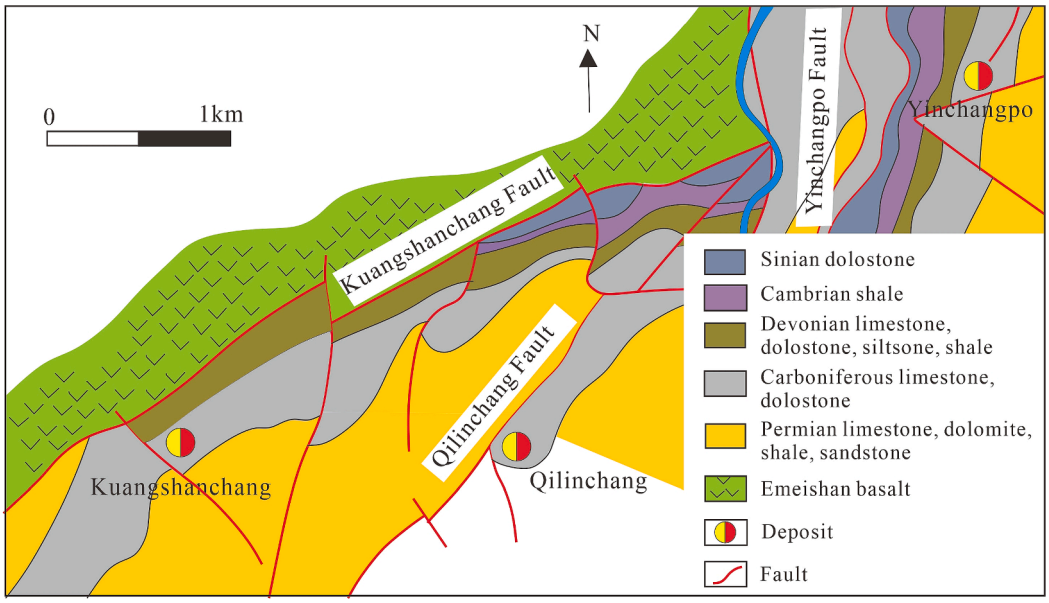

Fig. 2. Geological map of the Huize Pb-Zn deposit (modified after Han et al., 2012).

fault, and the north-west Ziyun-Yadu fault (Liu and Lin, 1999; Han, et al., 2012; Zhou et al., 2014; Zhang et al., 2017). The Yangtze Block consists of Paleoproterozic to early Neoproterozic basement complexes that include lower crystalline basement and upper folded metamorphic basement and Late Neoproterozic to Cenozoic cover sequences (Qiu et al., 2000; Zhou et al., 2018a). The basement rocks in this region consist of the Kangding, Dahongshan, and Kunyang Groups, which are sandstone, siltstone, slate, shale, dolostone, and minor tuffaceous volcanic rocks (Oyebamiji et al., 2020b). The cover sequences are composed of submarine carbonate, clastic sedimentary sequences, and terrigenous sedimentary sequences (Yan et al., 2003; Bao et al., 2017). The main ore-hosting strata of the Pb-Zn deposits in the region include dolostone of the Sinian Dengying, Lower Cambrian Maidiping, and Carboniferous Baizuo Formations. The deposits hosted by these three Formations account for ~ 62% of the total number of deposits and ~ 70% of the reserves of Pb-Zn resources in the SYG district (Fig. 1c) (Wu, 2013). Major structures consist of NS-trending, NE-trending, and NW-trending faults, which not only control the distribution of Pb-Zn deposits, but also control the petrographic distribution, in particular of the carbonates in the SYG province (Zhou et al., 2013b; Zhang et al., 2015). Hydrothermal dolomitization is widespread in the SYG district, which is closely related to sulfide ore bodies (Han et al., 2007; Tan et al., 2022). The host rocks all have different degrees of dolomitization, from gray coarse-grained massive dolomitization, white coarse- to fine-grained thick layered dolomitization, to light gray fine-grained vein-type dolomitization. Permian Emeishan basalt is the most widespread magmatic rock in the Yangtze Block (Zhou et al., 2013a). The Neoproterozoic to Lower Permian carbonate rocks hosts Pb-Zn deposits, which are all overlain by Middle Permian Emeishan flood basalts (Liu and Lin, 1999; Zhou et al., 2013c).

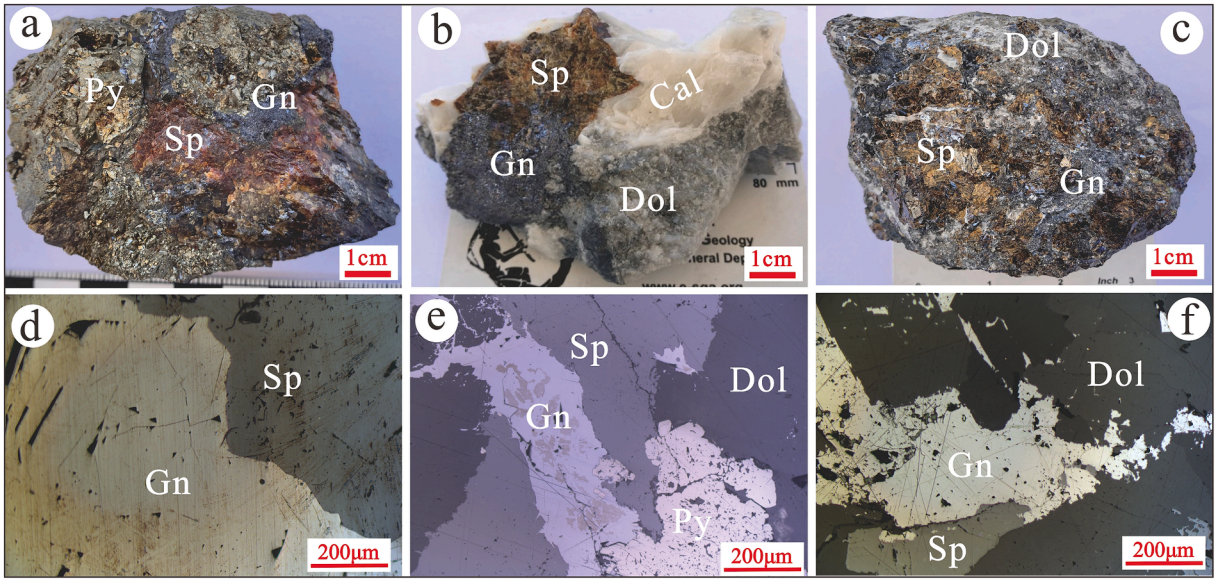

Fig. 3. Photographs at the hand-sample and microscopic scale of specimen from the Huize Pb-Zn deposit. (a) Massive sulfide ore, sphalerite and galena veins and veinlets within massive pyrite (b) Vein-like ores composed of sphalerite, galena, calcite and dolostone; (c) Disseminated sulfide ore, sphalerite and galena distributed in dolostone; (d) Coarse-grained galena coexists with sphalerite; (e) Coarse-grained pyrite coexists with sphalerite that cross-cutted by galena; (f) Coarse-grained galena coexists with sphalerite enclosed in dolomite. Gn = galena; Sp = sphalerite; Py = pyrite; Dol = dolomite; Cal = Calcite.

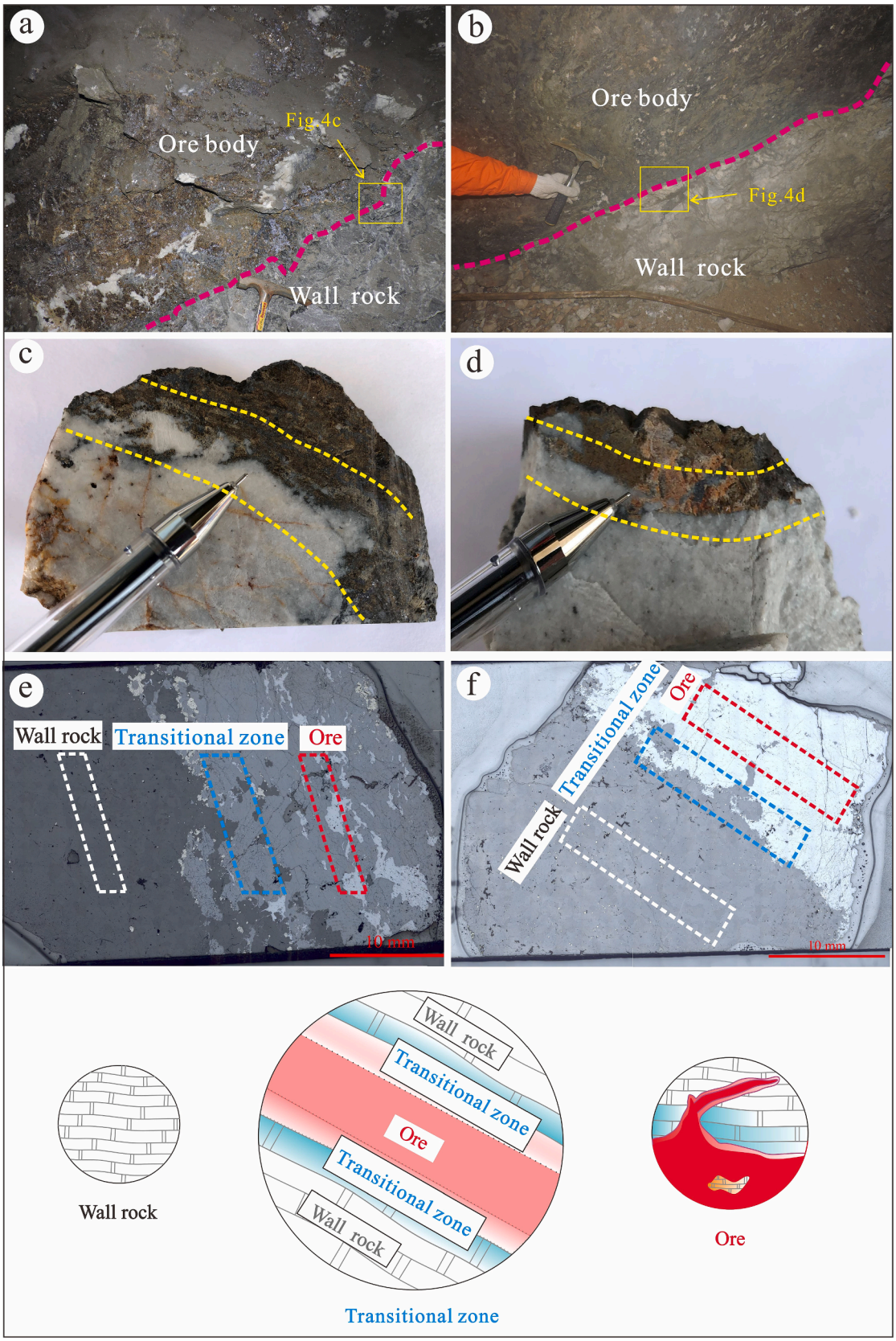

Fig. 4. Sample characterization and the research object. (a-b) Photographs of field, the contact boundary between sulfide ore body and wall rock is clear and the contact zone is easily identified; (c-d) Photographs of hand specimen scale, the contact boundary can be transitional or abrupt; (e-f) Photographs of microscope, three zones were divided on the thin section, from ore, transitional zone, to wall rock, and the different minerals in the three zones are used as the research object of this paper.

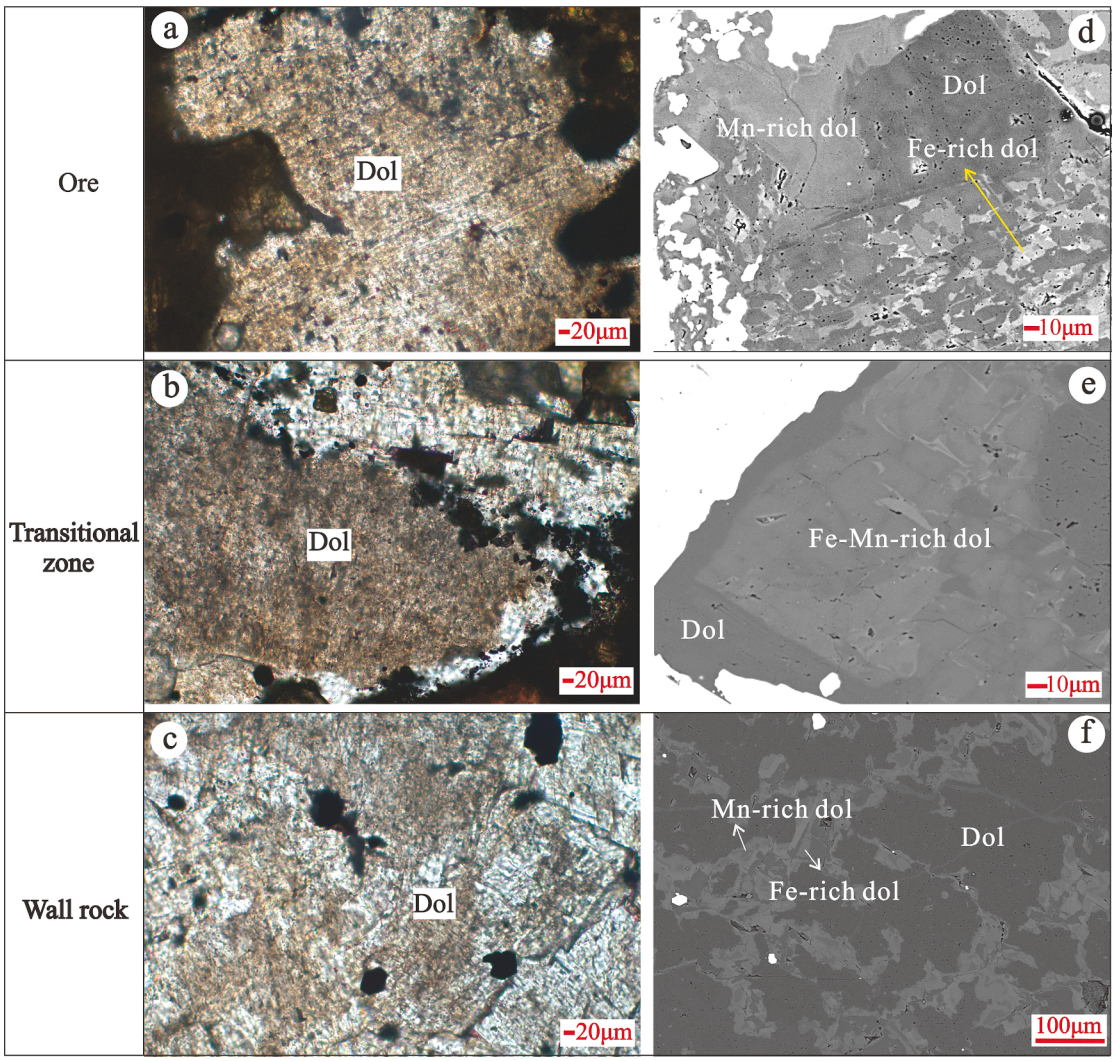

Fig. 5. Microscope transmitted light photographs (a-c) and scanning electron microscopy (SEM) backscattered electron images (d-f) of dolomite from the ore, transitional zone, to the wall rock in the Huize Pb-Zn deposit. (a, d) Characteristics of dolomite at the same location in the ore, dolomite is characterized by irregular metasomatism relics of dolomite by Fe- and Mn-rich dolomite; (b, e) Characteristics of dolomite at the same location in the transitional zone, dolomite has core-rim texture with dolomite in the core and Fe- and Mn-rich dolomite in the rim; (c, f) Characteristics of dolomite at the same location in the wall rock, Fe- and Mn-rich dolomite occur as veins between dolomite grains. Gn: galena; Sp: sphalerite; Dol: dolomite.

3. Geology of Huize deposit

The Huize Pb-Zn deposit is located in the central part of the SYG metallogenic province. There are more than 50 orebodies of various sizes in the Huize ore district. This deposit includes the Kuangshanchang (42 orebodies), Qilinchang (8 orebodies), and Yinchangpo sub-districts (Han et al., 2007), and is mainly controlled by the NE-trending faults (Fig. 2). The age of the host rocks ranges from Sinian (Ediacaran) to Permian (Zhou et al., 2001). Among them, the Lower Carboniferous Baizuo Formation is the most important ore-hosting rock, which is composed of gray, medium- and coarse-crystalline dolostone. The ore bodies are layered, lenticular, saccular, and vein-like (Zhou et al., 2001; Han et al., 2007; Li et al., 2007b). The ores are massive, vein-like, reticulated vein-like and disseminated. The massive ores are composed of sphalerite, pyrite, galena aggregates and minor dolomite (Fig. 3a). The vein-like ores are characterized by dolomite and calcite veins crosscutting the assemblages of sphalerite and galena (Fig. 3b). The disseminated ores show fine-grained sphalerite and galena distributed in the dolomite matrix (Fig. 3c). The ore minerals mainly include sphalerite, galena, and pyrite, and the gangue minerals are dolomite, Fe-rich dolomite, and calcite (Fig. 3a-c). Sphalerite is present as euhedral-subhedral crystals coexisting with galena or crosscut by galena (Fig. 3d-e). Galena always shows a “pressure shadow” texture (Fig. 3d). Pyrite shows a subhedral coarse-grained crystal and is strongly fractured and deformed (Fig. 3e). Wall rock alteration includes dolomitization, calcification, pyritization, and silicification. Mineralization-alteration zoning from ore body to wall rock is Pb-Zn ore → mineralized coarse-grained dolostone → gray coarse-grained dolostone → beige coarse-grained dolostone. The boundary between Pb-Zn ore and dolostone is obvious, and a small amount of galena with fine veins is distributed in dolostone. The carbonate alteration is closely associated with Pb–Zn mineralization (Han et al., 2012).

4. Samples and analytical methods

4.1. Sample collection

Five samples were collected from the mining adits at 1199–1404 m. In the field, the contact boundary between the sulfide ore body and wall rock is clear and the contact zone is easily identified (Fig. 4a, b). The samples were collected perpendicular to the contact zone. On the hand specimen scale, the contact boundary can be transitional or abrupt

Table 1
Major element (in wt%) of dolomite from the ore, transitional zone, and the wall rock in the Huize Pb-Zn deposit.

Sample	Location	CaO	MgO	FeO	MnO	BaO	Na_2O	SrO	Al_2O_3	CO_2	Total
Kb-2	Ore	28.86	18.18	4.687	0.756	–	0.032	–	–	47.68	100.21
		28.67	18.60	4.062	0.513	–	–	–		47.68	99.52
		28.67	18.52	4.129	0.782	–	–	–	–	47.68	99.80
		28.85	17.17	5.514	0.693	–	–	–	–	47.68	99.94
		29.07	18.91	3.993	0.714	–	0.027	–	–	47.68	100.42
	Transitional zone	28.99	19.44	1.025	1.245	–	–	–	–	47.68	98.39
		29.49	19.98	0.982	1.467	–	–	–	–	47.68	99.62
		29.62	19.56	1.827	1.321	–	0.027	0.034	0.032	47.68	100.10
		29.55	19.49	1.330	1.369	–	–	0.038	–	47.68	99.49
		29.73	20.84	0.891	1.336	–	–	–	0.027	47.68	100.56
		29.77	20.41	0.954	1.289	0.04	–	–	–	47.68	100.15
	Wall rock	30.70	22.00	0.122	0.031	–	0.03	0.061	–	47.68	100.63
		29.35	22.28	0.047	0.030	–	–	0.068	–	47.68	99.46
		30.67	21.90	0.323	0.087	0.046	–	0.056	–	47.68	100.77
		30.87	22.12	0.083	0.015	–	0.026	–	–	47.68	100.81
Ql-8	Ore	28.81	12.77	13.403	1.755	–	0.057	0.044		47.68	104.56
		28.43	12.61	12.842	1.576	–	–	–	–	47.68	103.19
		29.01	12.42	13.352	1.513	–	0.04	–	–	47.68	104.04
		29.03	12.95	12.496	1.747	–	–	–	–	47.68	103.93
		28.67	12.90	12.064	1.556	–	0.039	–	–	47.68	102.92
	Transitional zone	29.73	21.62	0.135	0.295	–	0.03	–	0.035	47.68	99.52
		30.34	21.98	0.057	0.252	–	–	0.075	0.023	47.68	100.42
		28.97	13.87	10.192	1.709	–	–	0.077	0.059	47.68	102.59
		29.09	14.74	8.828	1.764	–	–	–	–	47.68	102.13
		30.30	21.47	0.177	0.879	–	–	–	0.018	47.68	100.55
		29.42	21.07	0.732	0.605	–	–	0.06	0.018	47.68	99.59
	Wall rock	29.00	13.77	10.919	1.653	–	–	–	–	47.68	103.05
		29.21	14.87	9.326	1.683	0.046	–	0.043	–	47.68	102.88
		31.03	22.08	0.160	–	–	–	0.083	0.079	47.68	101.12
		29.22	14.91	9.202	1.624	–	–	–	–	47.68	102.65
		29.01	13.62	10.660	1.796	–	–	–	0.023	47.68	102.80
		30.38	22.17	0.063	–	–	–	–	–	47.68	100.34
Kb-3	Ore	29.30	19.36	2.529	1.722	–	0.051	0.057	–	47.68	100.70
		31.14	20.93	0.150	0.178	–	–	–	0.016	47.68	100.11
		29.66	20.25	0.125	0.176	–	0.082	–	–	47.68	97.99
		30.20	21.34	0.168	0.146	–	–	–	–	47.68	99.57
		30.70	21.21	0.133	0.150	–	–	–	0.018	47.68	99.92
	Transitional zone	30.26	21.17	0.032	0.163	–	–	0.037	–	47.68	99.37
		30.84	21.83	0.014	0.151	–	–	–	0.032	47.68	100.56
		30.09	21.97	0.029	0.139	–	–	0.046	0.033	47.68	99.99
		30.81	21.54	0.023	0.134	–	–	–	0.018	47.68	100.21
		30.84	21.81	0.017	0.154	–	–	–	0.023	47.68	100.55
		30.63	21.91	0.022	0.168	–	0.041	–	–	47.68	100.47
		30.69	21.61	0.022	0.176	–	–	–	0.027	47.68	100.20
		30.62	22.35	0.021	0.157	0.067	–	0.048	–	47.68	100.94
Kb-4	Ore	29.34	19.45	2.420	1.379	–	–	–	–	47.68	100.29
		29.38	20.80	0.915	1.249	0.037	–	–	–	47.68	100.07
		29.68	21.74	0.391	1.089	–	–	–	–	47.68	100.61
		28.25	21.52	0.083	0.215	–	0.033	–	–	47.68	97.78
		29.99	21.44	0.240	0.829	–	0.026	–	–	47.68	100.21
	Transitional zone	31.17	22.16	–	–	–	–	0.045	–	47.68	101.09
		29.82	22.26	0.030	0.471	–	0.045	0.037	–	47.68	100.34
		30.71	21.85	0.016	–	–	–	0.072	–	47.68	100.34
		29.55	19.45	–	0.310	–	0.064	–	0.018	47.68	97.10
		30.70	22.18	–	–	–	–	–	–	47.68	100.58
	Wall rock	30.83	21.88	0.016	0.035	–	0.067	–	0.032	47.68	100.54
		30.64	21.98	–	0.179	–	–	0.042	–	47.68	100.57
		31.17	22.16	–	–	–	–	0.045	–	47.68	101.09

Note "-" is below the detection limit.

(Fig. 4c, d). Thin sections were made along the contact zone. Three zones were divided on the thin section, from the ore, transitional zone, to the wall rock (Fig. 4e, f). A comparative study of the mineralogical characteristics, in-situ trace element, S and Pb isotopic compositions of dolomite, sphalerite and galena on the three different zones was carried out.

4.2. Scanning electron microscopy and electron probe microanalyzer analysis

Scanning electron microscopy (SEM) and electron microprobe analysis (EMPA) were completed at the State Key Laboratory of Ore Deposit Geochemistry (SKLODG), Institute of Geochemistry, Chinese Academy of Sciences (IGCAS). The JSM-7800F field emission SEM was used to identify mineral texture and association, whereas EPMA-1600 was used to analyze major elements of dolomite. EPMA was carried out using an accelerating voltage of 15 kV, a current of 20nA, and a spot diameter of 10 μm. ZAF software was used to correct matrix effects. Element content was calibrated by SPI (Structure Probe, Inc., West Chester, PA) dolomite standard. Average detection limits are 116 ppm for Fe, 111 ppm for Mn, 310 ppm for Ba, 258 ppm for Na, 249 ppm for Sr, 151 ppm for Mg, 149 ppm for Al, and 57 ppm for Ca.

4.3. LA-ICP-MS analysis

The contents of trace elements in dolomite were analyzed at the SKLODG, IGCAS, using an LA-ICP-MS composed of GeoLasPro 193 nm ArF excimer laser ablation system and Agilent 7700X ICP-MS. Elemental concentration was calibrated by NIST SRM 612, and EPMA Ca content was used as an internal standard. The USGS carbonate pellet Macs-3 (Jochum et al., 2012) was used as a monitoring sample. The isotopes of 17 elements were measured: ^{51}V, ^{52}Cr, ^{55}Mn, ^{57}Fe, ^{59}Co, ^{60}Ni, ^{65}Cu, ^{66}Zn, ^{71}Ga, ^{74}Ge, ^{75}As, ^{88}Sr, ^{107}Ag, ^{114}Cd, ^{115}In, ^{118}Sn, ^{121}Sb. The 5-Hz frequency and 44-μm beam spot were used for laser ablation. The analysis was composed of 18 s background, 60 s sample ablation and post-ablation gas clean. The external standard and monitoring materials were analyzed once for every 15 unknown analyses. Spectrum data were reduced by ICPMSDataCal software (Chen et al., 2011).

4.4. In situ S isotope analysis

In situ sulfur isotopes were analyzed by a Nu Plasma III MC-ICP-MS (Nu Instruments) coupled to a RESOlution-155 ArF193-nm laser ablation system (Australian Scientific Instruments) at the SKLODG, IGCAS. Analytical procedures have been described in Bao et al. (2016), Bao et al. (2017) and Chen et al. (2019), and are summarized here. Pseudo-medium resolution mode (Millet et al., 2012) was used to resolve polyatomic interferences of ^{16}O–^{16}O and ^{16}O–^{18}O on ^{32}S and ^{34}S, respectively. The mass separation was calculated as 0.3333. The source slit was adjusted to medium (0.05 mm) using the alpha slit. Sphalerite was ablated using 20 s baseline time, 40 s ablation time, 40 s wash time, 40–60 μm spot size, 5 Hz repetition rate and 2–3 J/cm^2 energy density. The sulfur isotope composition was calibrated using GBW07270 ($\delta^{34}S_{V\text{-}CDT}$: −5.5‰). The analysis quality was monitored by LZY08 ($\delta^{34}S_{V\text{-}CDT}$: 9.9‰), with an external precision (2SD) of ± 0.5 ‰.

4.5. In situ Pb isotope analysis

In situ Pb isotopic composition of galena was analyzed at the State Key Laboratory of Continental Dynamics, Northwestern University, using an LA-MC-ICP-MS system and a membrane desolvation device. The LA-MC-ICP-MS was composed of a 193 nm RESOLoution M-50 laser system and a Nu Plasma II type MC-ICP-MS (Nu Ins, UK). A Cetac's Aridus II type Desolvation Nebulizer (Ardus II, Ceac, USA) was used in the sample introduction. Detailed analytical procedures can be referred to Bao et al. (2016) and Yuan et al. (2015). The analyses are carried out using an ablation time of ~ 50 s, laser frequency of 3 Hz, and a stripping spot beam of 9–100 μm. The final Pb isotope ratio was obtained by normalizing the original data to the standard NIST SRM 981. The repeated analyses of the standard NIST SRM 610 yield an external precision of ± 0. 01‰.

5. Results

5.1. Petrography

At the hand specimen scale, the contact boundary between gray-white dolostone and Pb-Zn ore is obvious. The dolostones are distributed in the ore, transitional zone, and wall rock, and are mainly composed of dolomite. The dolomites in the three zones are coarsely crystallized, formed by recrystallization or dolomitization in some commodious spaces (Fig. 5a-c). Fe- and Mn-rich dolomite are obviously different from common dolomite in BSE images (Fig. 5d-f).

In the ore, a few dolostones are enclosed by the ore body (Fig. 4c-f). The dolomites all have unequal grain texture (grain size 0.5–1.5 mm), enclosed in sphalerite, with irregular crystal edges (Fig. 5a). The dolomite is characterized by anhedral dolomite relics metasomatized by Fe- and Mn-rich dolomite (Fig. 5d), with obvious recrystallization phenomenon.

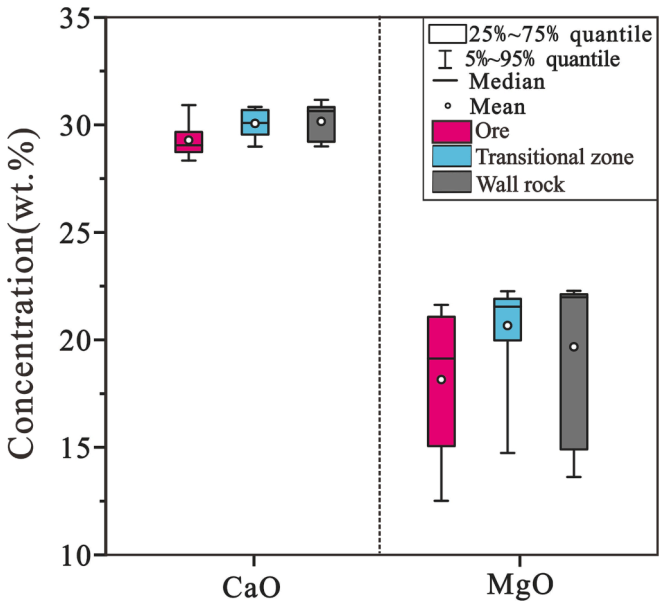

Fig. 6. Box plots of CaO and MgO in dolomite of the Huize Pb-Zn deposit.

In the transitional zone, the contact boundary between the sulfide ore body and wall rock is clear and the contact zone is easily identified (Fig. 4a, b). The dolomites exhibit growth zones with a clear core and relatively cloudy encasing cortices (Fig. 5b). The dolomites have core-rim texture with dolomite in the core and Fe- and Mn-rich dolomite in the rim (Fig. 5e).

In the wall rock, the dolomites have complete mineral crystal form, heteromorphic saddle shape. Some dolomites have tiny cracks and dissolution features (e.g. holes, Fig. 5c). Fe- and Mn-rich dolomite occur as veins between dolomite grains, and a few fine-grained pyrite are distributed in dolomite (Fig. 5f).

5.2. Major and trace elements in dolomite

EPMA analyses show that dolomite is composed of mainly Ca, Mg, Fe, and Mn (Table 1) (Tan et al., 2022). The CaO and MgO contents in dolomite from ore, transitional, and wall rock zones are relatively stable, ranging from 28.4 to 31.2 wt% and from 12.4 to 22.4 wt%, respectively. The FeO and MnO contents are various, with ranges of 0.014 to13.4 wt% and 0.02 to1.8 wt%, respectively. The BaO, Na_2O, SrO, and Al_2O_3 are mostly below the detection limit.

The dolomite in ores has lower CaO and MgO contents (average 29.3 wt% and 17.2 wt%) than those in the transitional zone and wall rock. From ore, transitional zone to wall rock, dolomite shows a trend of increasing Ca and Mg concentration (Fig. 6). The concentrations of Ba, Na, Sr, and Al show no obvious variation between these three zones.

The LA-ICP-MS analyses (Table 2) show that the dolomite is relatively rich in Mn, Fe, Zn, and Si, with averages of 3625 ppm, 13185 ppm, 3106 ppm, and 71 ppm, respectively (Tan et al., 2022). The concentrations of Ga, Ge, Ag, In, and Sb are relatively low, with averages of 0.18 ppm, 0.26 ppm, 0.66 ppm, 0.01 ppm, and 1.26 ppm, respectively. From the ore, transitional zone, to the wall rock, Mn, Fe, In, V concentrations gradually decrease (Fig. 7). The Cu, Zn, Ag, Cd, Co, and Ni contents are higher in the ore (average 1.51 ppm, 8958 ppm, 0.88 ppm, 14.57 ppm, 0.35 ppm, and 3.04 ppm, respectively) than in transitional zone and wall rock. The contents of As, Sr, Sb, Sn, Ge, and Cr are similar in the three zones.

The contents of REE in dolomite are relatively low (average 3.86 ppm) but variable (0.53 to 10.44 ppm) (Table 3), with differences in maximum and minimum contents up to one order of magnitude (Tan et al., 2022). We have supplemented the REE pattern of unmineralized

Table 2
LA-ICP-MS trace element results (in ppm) of dolomite from the ore, transitional zone, and the wall rock in the Huize Pb-Zn deposit.

Sample and location		Mn	Fe	Co	Ni	Cu	Zn	Ga	Ge	As	Sr	Ag	Cd	In	Sn	Sb	V	Cr
Kb-2	max	11,070	40,906	1.75	12.7	1.13	8672	0.13	0.15	15.0	109	0.23	18.2	0.008	0.76	0.60	83.9	8.33
Ore	min	6997	8593	0.03	0.19	–	195	0.02	–	0.09	67.7	–	0.32	–	0.07	–	7.84	1.24
(N = 10)	mean	8814	21,171	0.70	5.39	–	3150	0.04	–	1.77	91.1	–	2.89	–	0.35	–	31.1	3.44
	S.D.	1163	10,397	0.63	5.04	–	2899	0.03	–	4.65	12.4	–	5.45	–	0.26	–	26.0	2.53
Kb-2	max	10,650	37,890	0.23	1.38	10.2	994	0.09	0.23	8.43	106	35.1	1.25	0.007	0.68	32.2	15.1	29.5
Transitional zone	min	988	2675	0.02	0.14	0.02	11.2	–	–	0.14	29.2	–	0.05	–	0.15	–	0.78	1.58
(N = 9)	mean	6162	14,605	0.09	0.70	1.24	143	–	–	1.25	79.9	–	0.29	–	0.35	–	6.80	7.36
	S.D.	3339	11,396	0.06	0.41	3.35	321	–	–	2.70	29.1	–	0.37	–	0.18	–	4.88	9.02
Kb-2	max	536	1452	0.15	0.97	0.42	26.4	0.03	0.49	2.88	38.7	0.03	0.31	0.005	0.27	0.03	0.72	2.31
Wall rock	min	94.4	377	0.06	0.45	–	5.69	0.01	–	0.04	31.4	–	0.20	–	0.12	–	0.24	1.27
(N = 5)	mean	351	714	0.09	0.74	–	18.2	0.02	–	0.70	35.3	–	0.25	–	0.18	–	0.47	1.94
	S.D.	191	431	0.03	0.20	–	8.14	0.01	–	1.22	2.58	–	0.04	–	0.06	–	0.20	0.40
Ql-8	max	13,390	82,182	0.17	0.91	23.8	88,442	9.16	1.11	58.3	119	6.37	165	0.512	8.54	5.88	4.78	4.56
Ore	min	93.2	629	0.04	0.07	0.02	8.67	0.01	–	–	54.9	–	0.04	–	0.04	0.01	0.22	0.22
(N = 12)	mean	5624	23,949	0.09	0.41	2.52	9258	0.97	–	–	87.5	–	17.5	–	1.00	0.69	2.70	2.16
	S.D.	4490	27,681	0.04	0.22	7.05	26,392	2.72	–	–	20.9	–	49.1	–	2.51	1.75	1.45	1.17
Ql-8	max	13,524	176,741	1.99	12.9	16.5	185	0.32	1.20	2238	106	0.94	0.38	0.009	0.50	5.66	9.49	5.87
Transitional zone	min	103	555	0.02	–	0.01	8.91	–	–	0.10	58.5	–	–	–	0.07	–	0.24	0.44
(N = 16)	mean	6329	39,998	0.20	–	1.72	45.3	–	–	181	79.6	–	–	–	0.29	–	3.60	2.37
	S.D.	5333	47,141	0.52	–	4.56	43.4	–	–	596	14.3	–	–	–	0.13	–	3.29	1.57
Ql-8	max	11,493	56,336	0.20	0.77	0.77	57.9	0.62	0.50	104	103	0.06	0.35	0.008	0.47	0.16	4.98	4.05
Wall rock	min	900	5077	0.04	0.36	–	17.1	0.01	–	0.03	60.9	–	0.09	–	0.09	0.00	1.16	1.14
(N = 8)	mean	5120	24,079	0.11	0.53	–	32.8	0.18	–	13.6	79.0	–	0.22	–	0.27	0.05	2.80	2.68
	S.D.	3909	17,643	0.05	0.14	–	14.2	0.21	–	36.7	14.7	–	0.09	–	0.14	0.05	1.45	0.88
Kb-3	max	2125	3391	1.08	17.6	6.48	49,693	0.08	0.25	0.79	95.5	0.60	90.0	0.018	0.57	0.53	88.9	2.12
Ore	min	771	424	0.09	0.80	0.05	606	0.03	–	–	25.3	–	0.32	–	0.43	–	1.60	0.78
(N = 3)	mean	1369	1950	0.49	6.65	2.23	17,922	0.05	–	–	54.9	–	32.7	–	0.52	–	32.4	1.44
	S.D.	691	1486	0.52	9.53	3.68	27,552	0.03	–	–	36.3	–	49.7	–	0.07	–	49.0	0.67
Kb-3	max	6488	10,618	0.14	0.94	0.53	24.7	0.06	0.33	5.49	125.4	0.19	0.29	0.012	0.51	0.24	6.40	5.23
Transitional zone	min	64.7	65.9	0.01	–	–	–	–	–	0.04	24.1	–	–	–	0.25	–	0.16	0.16
(N = 13)	mean	1310	1489	0.06	–	–	–	–	–	0.79	83.3	–	–	–	0.38	–	2.03	1.12
	S.D.	1620	2868	0.05	–	–	–	–	–	1.44	37.6	–	–	–	0.07	–	1.90	1.40
Kb-3	max	1140	1832	0.10	0.83	0.04	13.7	0.04	0.19	0.69	62.1	0.01	0.34	0.001	0.51	0.06	0.95	1.55
Wall rock	min	152	345	0.05	0.33	–	4.06	0.01	–	0.42	41.5	–	0.12	–	0.35	0.01	0.07	0.26
(N = 5)	mean	380	749	0.07	0.58	–	6.55	0.02	–	0.52	49.1	–	0.24	–	0.44	0.03	0.46	0.89
	S.D.	426	613	0.02	0.23	–	4.06	0.01	–	0.10	8.27	–	0.09	–	0.08	0.02	0.40	0.52
Kb-4	max	1080	258	0.07	0.43	1.46	47,838	0.07	0.41	0.53	82.9	8.93	61.6	0.056	0.61	0.77	0.49	1.05
Ore	min	117	144	0.01	0.38	0.11	34.5	0.02	0.24	0.29	54.3	–	0.28	–	0.42	0.06	–	0.72
(N = 3)	mean	483	213	0.03	0.41	0.64	18,264	0.04	0.34	0.39	64.6	3.13	24.6	–	0.54	0.32	–	0.83
	S.D.	522	60.9	0.03	0.03	0.72	25,842	0.03	0.09	0.13	15.9	5.02	32.6	–	0.10	0.39	–	0.18
Kb-4	max	3079	644	0.12	0.69	0.19	11.8	0.04	0.44	0.57	93.2	0.46	0.33	0.006	0.75	0.37	3.32	3.41
Transitional zone	min	540	212	0.02	0.00	–	–	–	–	–	50.9	–	0.00	–	0.11	–	0.38	0.37
(N = 11)	mean	1432	399	0.05	0.31	–	–	–	–	–	73.7	–	0.13	–	0.34	–	1.25	1.43
	S.D.	872	130	0.03	0.18	–	–	–	–	–	15.6	–	0.09	–	0.22	–	0.87	0.82
Kb-zk	max	401	10,306	0.28	2.42	0.28	3161	0.13	2.25	185	56.1	0.05	114	0.154	0.32	87.3	1.68	3.12
Transitional zone	min	89.9	462	0.03	0.63	–	115	–	–	0.76	35.8	–	1.49	–	0.12	0.08	0.12	0.53
(N = 10)	mean	238	2195	0.07	1.02	–	1188	–	–	33.3	46.9	–	27.0	–	0.21	12.3	1.06	1.93
	S.D.	122	2975	0.08	0.55	–	1225	–	–	59.5	5.34	–	35.0	–	0.07	26.7	0.53	1.03
Kb-zk	max	252	817	0.04	0.69	0.23	1441	0.01	0.27	4.46	51.6	0.06	5.26	0.004	0.22	0.65	2.40	4.27
Wall rock	min	47.5	183	0.02	0.45	–	4.35	–	–	0.24	42.6	–	0.18	–	0.15	0.04	–	1.54
(N = 5)	mean	140	423	0.03	0.55	–	391	–	–	1.39	46.6	–	1.80	–	0.17	0.24	–	2.60
	S.D.	83.3	287	0.01	0.09	–	604	–	–	1.77	3.57	–	2.21	–	0.03	0.26	–	1.09

Note "-" is below the detection limit.

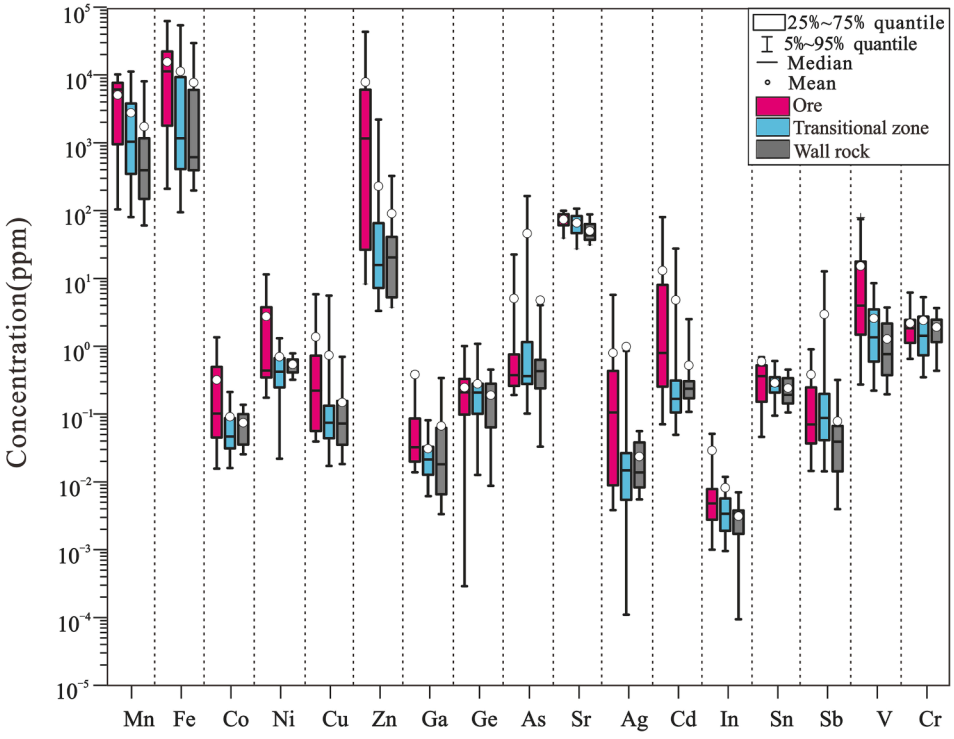

Fig. 7. Box plots of trace elements in dolomite of the Huize Pb-Zn deposit (Tan et al., 2022).

dolomite (Tan et al., 2022), showing the characteristics of LREE enrichment, HREE relative deficit, and negative Ce and Eu anomalies. The average REE concentration of dolomite in the ore is lower than transitional zone and wall rock, and the LREE contents are obviously depleted in three different zones relative to unmineralized carbonates (Fig. 8). From the ore, transitional zone, to the wall rock, negative Ce anomaly gradually weakens.

5.3. *In situ sulfur isotopic composition of sphalerite*

The $\delta^{34}S$ values of sphalerite in the transitional zone range from −2.8 to + 9.8 ‰, whereas those of sphalerite in the ore vary from + 5.3 to + 17.7 ‰ (Table 4) (Fig. 9a). The $\delta^{34}S$ values of one sphalerite grain in the transitional zone from core to rim range from + 1.2 to + 5.3 ‰, those of another sphalerite grain in the transitional zone from core to rim range from + 7 to 9.7 ‰ (Fig. 9b-c).

5.4. *In situ Pb isotopic compositions of galena*

The in situ Pb isotopic compositions of galena are listed in Table 5. Galena in the ore has $^{206}Pb/^{204}Pb$ ratios ranging from 18.474 to 18.484, $^{207}Pb/^{204}Pb$ ratios ranging from 15.715 to 15.722, and $^{208}Pb/^{204}Pb$ ratios ranging from 38.889 to 38.914. Galena in the transitional zone has $^{206}Pb/^{204}Pb$ ratios of 18.487 to 18.502, $^{207}Pb/^{204}Pb$ ratios of 15.730 to 15.739, and $^{208}Pb/^{204}Pb$ ratios of 38.938 to 38.982. Galena in wall rock has $^{206}Pb/^{204}Pb$, $^{207}Pb/^{204}Pb$, and $^{208}Pb/^{204}Pb$ ratios of 18.497 to 18.505, 15.741 to 15.744, and 38.986 to 39.003, respectively. In general, from the ore, transitional zone, to the wall rock, the Pb isotopic compositions gradually increase (Fig. 10).

6. Discussion

6.1. *Constraints on changes in fluids composition and physiochemical conditions from elemental composition of dolomite*

The formation of hydrothermal metal deposits includes the source, migration, and precipitation of ore-forming materials. Understanding the element transportation and precipitation is critical for the mineralization mechanism. The increased Ca and Mg and decreased Mn, Fe, In, and V contents in dolomite from the ore, transitional zone, to the wall rock (Fig. 7) indicated that the ore-forming fluids constantly exchange elements with dolomite. The ionic radii of Mn and Fe are close to those of Mg (Wogelius et al., 1992), and the larger ionic radius like Ca will be replaced by smaller ionic radius like In and V according to ionic radius rule (Chen et al., 2013; Frondini et al., 2014), which makes it easy for Mn, Fe, In, and V to replace Ca^{2+} and Mg^{2+} in dolomite. The concentration of elements (e. g. Mn, Fe, etc) in the solution will be increased during the dolomitization reaction (Wogelius et al., 1992). The dolostone is continuously metasomatized by fluids rich in Mn, Fe, In, V, and the elements in the fluids are consumed due to partition into the dolomite. In addition, the higher contents of Cu, Zn, Ag, and Cd in the dolomite from the ore than the transitional zone and wall rock are consistent with the fluid migration from the ore to the dolostone. The intense mineralization in the reaction front will result in a higher concentration of ore-related elements in dolomite of the ore zone with eventual precipitation of these elements as sphalerite upon saturation. With the evolution of the fluids towards the wall rock, the mineralization is weakened and the remaining fluids contains low content of ore-forming elements, resulting in low content of these elements in the dolomite of the transitional zone and wall rock.

In carbonate minerals, REE is often isomorphically exchanged with Ca^{2+}, so REE is usually enriched in Ca-bearing minerals. REE and Ca^{2+} undergo isomorphism exchange, and the exchange degree is gradually enhanced with Ca^{2+} in dolomite gradually increases, resulting in the content of REE elements in the three zones also gradually increase (Figs. 6, 8). The ionic radius of $LREE^{3+}$ is closer to Ca^{2+} than $HREE^{3+}$, so LREE is easier to substitute Ca in the lattice and enter dolomite (Zhong and Mucci, 1995; Rimstidt et al., 1998). Therefore, the content of LREE is more likely to vary with the Ca content of the dolomite of the three zones. In addition, the LREE contents are obviously lower in dolomite from three zones relative to unmineralized dolomite, demonstrating that LREE depletion is the feature of ore-related dolomite which can be used

Table 3
LA-ICP-MS REE composition results (in ppm) of dolomite from the ore, transitional zone, to the wall rock in the Huize Pb-Zn deposit.

Sample and location		La	Ce	Pr	Nd	Sm	Eu	Gd	Tb	Dy	Ho	Er	Tm	Yb	Lu	ΣREE	LREE	HREE	LREE /HREE	La_N /Yb_N	δEu	δCe
Kb-2	max	0.25	0.78	0.09	0.49	0.14	0.03	0.13	0.02	0.22	0.05	0.17	0.03	0.15	0.03	2.31	1.77	0.79	3.23	2.91	0.78	1.33
Ore	min	0.06	0.23	0.03	0.14	0.05	0.001	0.03	–	0.07	0.02	0.07	0.01	0.05	0.01	0.92	0.53	0.28	1.36	0.44	0.07	0.96
(N = 10)	mean	0.16	0.47	0.06	0.3	0.08	0.01	0.09	–	0.13	0.03	0.1	0.02	0.1	0.01	1.57	1.08	0.49	2.28	1.35	0.41	1.15
	S.D.	0.05	0.16	0.02	0.11	0.03	0.006	0.03	–	0.04	0.01	0.03	0.01	0.03	0.01	0.45	0.36	0.14	0.62	0.72	0.2	0.11
Kb-2	max	0.60	2.00	0.17	0.73	0.16	0.03	0.23	0.06	0.45	0.1	0.34	0.06	0.34	0.06	4.16	3.61	1.63	6.66	7.20	0.76	1.59
Transitional zone	min	0.07	0.21	0.04	0.14	0.03	0.002	–	0.01	0.07	0.02	0.05	0.01	0.05	0.01	0.72	0.48	0.24	1.23	0.54	0.11	0.99
(N = 9)	mean	0.31	0.89	0.1	0.4	0.09	0.01	–	0.02	0.16	0.03	0.11	0.02	0.11	0.02	2.36	1.80	0.56	3.7	2.83	0.44	1.2
	S.D.	0.21	0.57	0.04	0.18	0.05	0.009	–	0.01	0.12	0.03	0.09	0.02	0.09	0.01	1.16	1.02	0.41	2.15	2.32	0.23	0.17
Kb-2	max	0.83	2.12	0.21	0.89	0.18	0.03	0.17	0.03	0.14	0.03	0.1	0.01	0.09	0.01	4.64	4.25	0.47	10.6	13.3	0.66	1.21
Wall rock	min	0.65	1.28	0.16	0.57	0.12	0.01	0.08	0.02	0.07	0.02	0.06	0.006	0.04	0.01	3.23	2.83	0.4	6.45	5.31	0.26	0.88
(N = 5)	mean	0.72	1.5	0.18	0.69	0.15	0.02	0.12	0.02	0.11	0.02	0.07	0.009	0.07	0.001	3.69	3.26	0.43	7.62	8.28	0.54	1.00
	S.D.	0.08	0.35	0.02	0.12	0.03	0.01	0.03	0.00	0.03	0.00	0.02	0.004	0.02	0.001	0.56	0.57	0.03	1.70	3.11	0.17	0.13
Ql-8	max	1.02	1.74	0.25	0.92	0.18	0.04	0.16	0.02	0.15	0.04	0.16	0.03	0.35	0.06	4.70	4.15	0.85	15.10	18.4	1.19	1.27
Ore	min	0.09	0.21	0.02	0.12	0.02	0.01	0.02	0.004	0.02	0.01	0.01	0.003	0.02	–	0.57	0.47	0.10	1.75	0.76	0.35	0.82
(N = 12)	mean	0.48	0.92	0.10	0.43	0.08	0.02	0.08	0.01	0.08	0.02	0.06	0.01	0.10	0.02	2.41	2.04	0.37	6.36	5.83	0.66	1.03
	S.D.	0.31	0.54	0.07	0.27	0.06	0.01	0.05	0.01	0.05	0.01	0.04	0.01	0.09	0.02	1.35	1.25	0.22	4.06	5.45	0.24	0.14
Ql-8	max	1.06	1.75	0.24	0.99	0.22	0.04	0.15	0.02	0.16	0.05	0.16	0.03	0.26	0.06	4.66	4.20	0.73	11.75	24.4	1.21	1.25
Transitional zone	min	0.05	0.15	0.02	0.04	0.02	0.004	0.01	0.003	0.03	0.01	0.02	0.005	0.02	–	0.53	0.32	0.15	0.74	0.18	0.27	0.73
(N = 16)	mean	0.44	0.88	0.11	0.44	0.09	0.02	0.07	0.01	0.08	0.02	0.07	0.01	0.10	0.02	2.36	1.98	0.39	5.59	5.93	0.62	1.01
	S.D.	0.31	0.54	0.07	0.31	0.06	0.01	0.04	0.01	0.04	0.01	0.04	0.01	0.07	0.02	1.34	1.28	0.17	3.43	6.79	0.25	0.15
Ql-8	max	1.34	3.36	0.40	1.32	0.29	0.05	0.16	0.03	0.16	0.03	0.12	0.02	0.16	0.03	7.01	6.42	0.59	11.78	10.2	0.80	1.31
Wall rock	min	0.26	0.65	0.07	0.28	0.05	0.01	0.06	0.01	0.08	0.02	0.07	0.01	0.08	0.01	1.70	1.32	0.38	3.47	1.72	0.36	0.99
(N = 8)	mean	0.95	2.27	0.25	0.96	0.17	0.03	0.12	0.02	0.12	0.03	0.08	0.01	0.11	0.02	5.14	4.63	0.51	8.91	6.81	0.64	1.14
	S.D.	0.40	0.96	0.11	0.38	0.08	0.01	0.04	0.01	0.03	0.00	0.02	0.00	0.02	0.01	1.98	1.93	0.06	3.27	3.25	0.14	0.11
Kb-3	max	0.94	1.18	0.26	1.01	0.25	0.07	0.2	0.04	0.34	0.07	0.27	0.03	0.2	0.03	4.75	3.65	1.11	3.29	3.42	1.26	0.8
Ore	min	0.12	0.29	0.07	0.23	0.08	0.01	0.02	0.01	0.07	0.02	0.06	0.01	0.06	0.01	1.06	0.8	0.26	2.95	1.51	0.31	0.56
(N = 3)	mean	0.62	0.87	0.17	0.67	0.17	0.04	0.12	0.03	0.25	0.05	0.18	0.02	0.14	0.02	3.35	2.54	0.81	3.12	2.74	0.73	0.69
	S.D.	0.44	0.5	0.1	0.4	0.08	0.03	0.09	0.02	0.15	0.03	0.11	0.01	0.08	0.01	2.00	1.52	0.48	0.17	1.07	0.48	0.12
Kb-3	max	1.82	3.41	0.54	2.5	0.5	0.11	0.63	0.08	0.55	0.11	0.29	0.04	0.24	0.04	10.44	8.53	1.91	7.12	9.97	0.98	0.95
Transitional zone	min	0.07	0.18	0.04	0.23	0.06	0.01	0.09	0.01	0.08	0.02	0.04	–	0.02	0.01	1.00	0.59	0.31	1.42	0.47	0.26	0.45
(N = 13)	mean	0.96	1.62	0.27	1.15	0.28	0.05	0.29	0.04	0.28	0.06	0.16	–	0.15	0.02	5.37	4.34	1.04	4.20	5.25	0.55	0.78
	S.D.	0.53	0.9	0.14	0.64	0.14	0.03	0.16	0.02	0.14	0.03	0.08	–	0.07	0.01	2.70	2.25	0.52	1.42	2.97	0.18	0.18
Kb-3	max	1.3	1.72	0.3	1.45	0.33	0.06	0.37	0.05	0.29	0.06	0.19	0.03	0.22	0.02	6.03	4.96	1.08	6.00	9.06	0.9	0.68
Wall rock	min	1.17	1.53	0.28	1.03	0.19	0.04	0.22	0.02	0.21	0.04	0.11	0.02	0.10	0.02	5.14	4.41	0.73	4.31	4.08	0.45	0.59
(N = 5)	mean	1.24	1.61	0.29	1.16	0.24	0.05	0.27	0.04	0.25	0.05	0.15	0.02	0.14	0.02	5.55	4.60	0.95	4.90	6.75	0.62	0.63
	S.D.	0.05	0.08	0.01	0.18	0.06	0.01	0.06	0.01	0.03	0.01	0.03	0.004	0.05	0.003	0.33	0.23	0.13	0.65	1.92	0.17	0.03
Kb-4	max	1.43	1.25	0.32	1.29	0.24	0.06	0.31	0.04	0.30	0.08	0.28	0.03	0.24	0.03	5.30	3.98	1.31	4.90	7.14	0.69	0.60
Ore	min	1.10	0.57	0.20	0.84	0.19	0.02	0.22	0.01	0.15	0.04	0.13	0.01	0.12	0.002	3.98	3.22	0.74	3.03	4.20	0.31	0.22
(N = 3)	mean	1.23	0.82	0.25	1.04	0.22	0.04	0.26	0.03	0.21	0.06	0.18	0.02	0.17	0.02	4.54	3.60	0.94	4.05	5.53	0.50	0.36
	S.D.	0.18	0.37	0.06	0.23	0.03	0.02	0.05	0.01	0.08	0.02	0.08	0.01	0.07	0.01	0.68	0.38	0.33	0.94	1.49	0.19	0.21
Kb-4	max	0.35	0.98	0.22	1.27	0.42	0.04	0.37	0.06	0.33	0.06	0.20	0.03	0.18	0.02	4.31	3.13	1.18	3.53	2.01	0.71	0.92
Transitional zone	min	0.16	0.28	0.04	0.19	0.06	0.01	0.06	0.01	0.10	0.02	0.09	0.01	0.07	0.01	1.19	0.77	0.42	1.70	1.21	0.24	0.71
(N = 11)	mean	0.23	0.52	0.10	0.50	0.16	0.02	0.15	0.02	0.16	0.04	0.12	0.02	0.11	0.02	2.17	1.54	0.63	2.34	1.59	0.50	0.82
	S.D.	0.06	0.25	0.07	0.38	0.13	0.01	0.10	0.01	0.08	0.01	0.04	0.01	0.03	–	1.11	0.87	0.25	0.61	0.31	0.17	0.08
Kb-zk	max	0.31	0.61	0.10	0.58	0.18	0.02	0.18	0.03	0.17	0.04	0.14	0.02	0.12	0.02	2.53	1.82	0.72	2.54	1.96	0.39	0.83
Transitional zone	min	0.19	0.30	0.04	0.22	0.06	0.02	0.06	0.01	0.10	0.02	0.09	0.01	0.08	0.01	1.22	0.83	0.39	2.11	1.61	0.79	0.81
(N = 10)	mean	0.23	0.44	0.07	0.38	0.11	0.02	0.11	0.02	0.13	0.03	0.11	0.02	0.10	0.02	1.78	1.24	0.54	2.28	1.56	0.54	0.83
	S.D.	0.05	0.13	0.03	0.16	0.05	0.00	0.04	0.00	0.03	0.00	0.02	–	0.01	–	0.52	0.41	0.12	3.50	2.85	0.22	0.91
Kb-zk	max	0.21	0.40	0.06	0.30	0.09	0.02	0.12	0.02	0.12	0.03	0.10	0.01	0.10	0.02	1.56	1.06	0.50	2.11	2.38	0.66	0.88
Wall rock	min	0.15	0.27	0.03	0.15	0.05	0.01	0.08	0.01	0.08	0.02	0.06	0.01	0.06	0.01	1.10	0.70	0.40	1.73	1.39	0.34	0.65
(N = 5)	mean	0.19	0.30	0.05	0.22	0.06	0.01	0.11	0.01	0.09	0.03	0.09	0.01	0.08	0.01	1.27	0.83	0.44	1.90	1.67	0.51	0.77
	S.D.	0.02	0.06	0.01	0.07	0.02	0.01	0.02	0.00	0.02	0.01	0.01	–	0.02	–	0.18	0.15	0.04	0.19	0.40	0.12	0.11

Note "-" is below the detection limit.

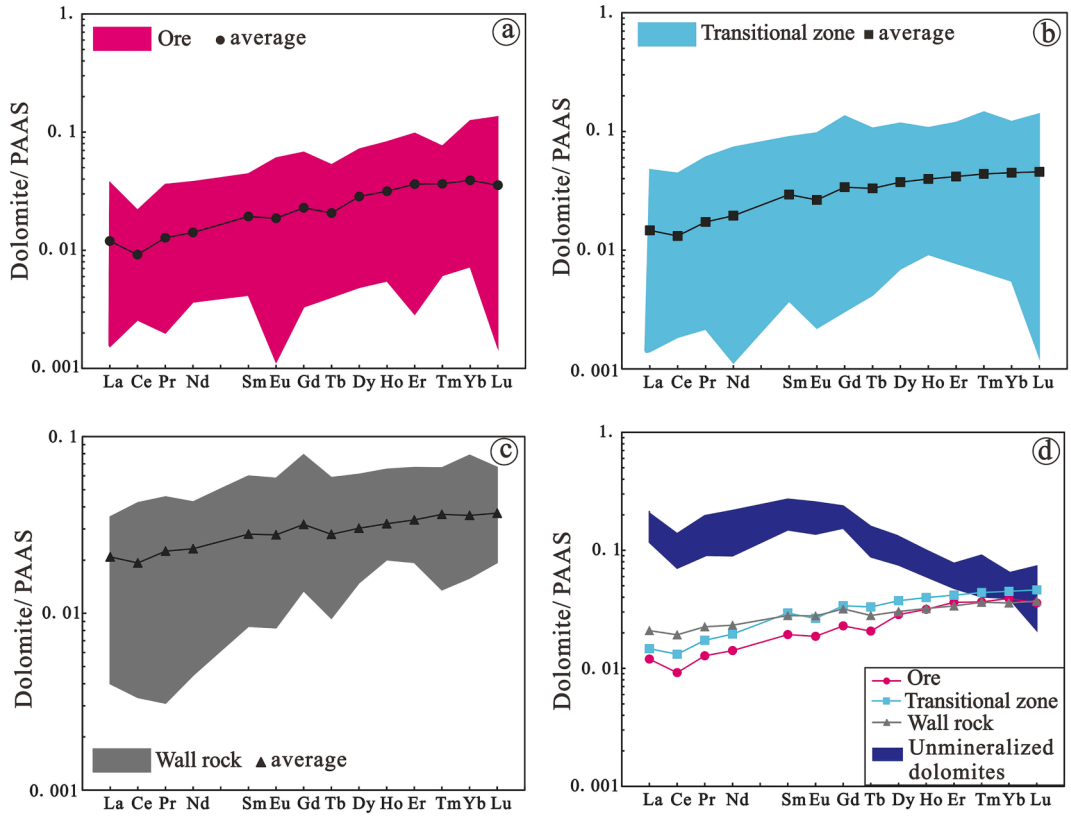

Fig. 8. PAAS (Post-Achaean Australian Shale) normalized REE patterns of dolomite in different zones of Huize Pb-Zn deposit (PAAS values are from Taylor and Mclennan, 1985) and unmineralized carbonates from the region (Tan et al., 2022).

Table 4
In situ S isotopic composition of sphalerite in the Huize Pb-Zn deposit.

NO.	Sample Location	Mineral	Experimental location	$\delta^{34}S_{CDT}$‰
Kb-2	1237 *m*	Sphalerite	Transitional zone	7.2
				2.7
				2.6
				3.6
				4.6
Kb-3	1199 *m*	Sphalerite	Ore	8.9
			Ore	17.7
			Core (transitional zone)	1.8
			Rim (transitional zone)	−2.8
Kb-4	1199 *m*	Sphalerite	Core (transitional zone)	5.3
			Middle (transitional zone)	3.3
			Rim (transitional zone)	1.2
			Ore	6.6
			Rim (transitional zone)	0.8
			Core (transitional zone)	5.9
Kb-zk	1249 *m*	Sphalerite	Ore	7.0
			Transitional zone	5.2
			Transitional zone	4.5
Ql-8	1237 *m*	Sphalerite	Core (transitional zone)	9.7
			Middle (transitional zone)	8.2
			Rim (transitional zone)	7.0
			Ore	9.8
			Ore	10.4
			transitional zone	4.1
			Ore	9.8

to discriminate ore-related hydrothermal dolomite from barren sedimentary dolomite (Fig. 8d). Such LREE-depleted dolomite can be interpreted as: 1) LREE scavenging by precipitation of certain micro-mineral phases with high REE-partition coefficients along the fluid pathway (Debruyne et al., 2016; Perry and Gysi, 2018; Rieger et al., 2022). The Phosphate minerals such as monazite or apatite possess high partition coefficients for REE, leading to fractionation of REE during the precipitation of other phases that formed in association with the hydrothermal carbonate (Debruyne et al., 2016). However, since there are no hydrothermal phosphate mineral phases present in the Huize Pb-Zn deposit, resulting in this scenario being unlikely. 2) REE contents inherited from the fluid-rock interaction (Lüders et al., 1993; Hecht et al., 1999). Some studies suggested that the hydrothermal dolomite associated with Mississippi-Valley-type (MVT) ore deposits may change the original REE patterns of host dolomite due to large amounts of Zn-Pb fluids (Anderson and Macqueen, 1982; Anderson, 1983; Banner et al., 1988a, b).The different REE patterns between hydrothermal dolomite (LREE-depleted) and unmineralized dolomite (LREE-enriched) suggest that fluid-rock ratios during mineralization were high, with significant volumes of fluids involved in Pb-Zn mineralization passing through the host dolomite and altering their REE patterns (Qing and Mountjoy, 1994). Therefore, the LREE elements of dolomite are inherited from the ore-forming fluids by fluid-rock interaction. 3) LREE are retained in the fluids through the formation of Cl^- complexes (Craddock et al., 2010; Magnall et al., 2016; Perry and Gysi, 2018). The ore-forming fluids in the Huize Pb-Zn deposit is a high salinity fluid containing chlorine (ca.3.2–22.7 wt% NaCl equiv) (Huang et al., 2004; Zhang, 2016). The chlorides are the strongest complexes with the REE due to the lowest charge/radius ratios (Migdisov et al., 2009; Williams-Jones et al., 2012; Perry and Gysi, 2018). Additionally, salinity exerts a significant influence on REE solubility and fractionation, leading to enhanced LREE retention in the fluids during carbonate precipitation. Consequently, LREE depletion in dolomite from the Huize Pb-Zn deposit can be caused by fluid-rock interaction and retention of Cl^- complexes.

The composition of REE represents the characteristics of ore-forming fluids, thus can be used to constrain the physicochemical conditions (Bau et al., 2003; Huang et al., 2010). Eu^{3+} is reduced to Eu^{2+}, Eu^{2+} ionic radius is 1.17 Å, which ion is larger than that of Ca^{2+} (1.0 Å) (Shannon, 1976). Divalent Eu would be rejected by the carbonate

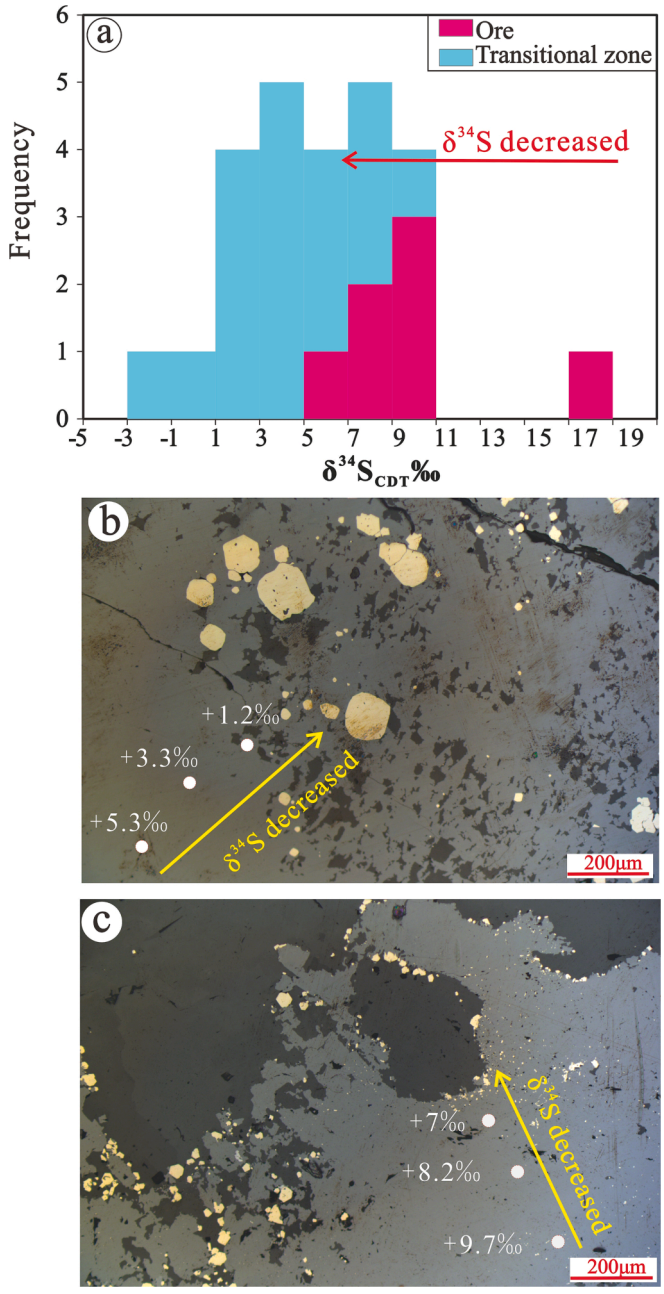

Fig. 9. (a) In-situ S isotopic variation of sphalerite in the hand specimen scale. (b-c) $\delta^{34}S$ values in sphalerite crystals from core to rim.

minerals lattice (Bau, 1991), and it's flowing in a fluid (Debruyne et al., 2016). This suggests that the decoupling of Eu from the other REEs in the mineral will result in the negative Eu anomaly of dolomite. Both unmineralized dolomite and hydrothermal dolomite show negative Eu anomalies (Fig. 8), indicating that negative Eu anomaly in the hydrothermal dolomite were inherited from the host dolomite during the dissolution and reprecipitation. However, physiochemical conditions during fluid migration seem to be more important for the development of Eu and Ce anomalies (Bau, 1991). The Eu anomaly is determined by temperature, pH, redox, and pressure, and the temperature is the main factor (Bau and Möller, 1992; Lüders et al., 1993). The temperature of fluids over 200 °C may change the Eu anomaly in carbonates (Bau, 1991). The homogenization temperatures of fluids inclusions in the hydrothermal dolomite vary from 86 to 163 °C (Zhang et al., 2017). Because the temperature of the fluids (less than 200 °C) is not high enough, the degree of negative Eu anomalies in the dolomite from ore, transitional zone, and wall rock has no obvious change.

Cerium (Ce) anomaly in carbonates has been proposed as an indicator of physiochemical conditions (Nagender Nath et al., 1997; Bolhar and Van Kranendonk, 2007; Komiya et al., 2008). The dolomites from the ore, transitional zone, to the wall rock are distributed in the field IIIb, indicating negative Ce anomaly (Fig. 11). This can be interpreted that Ce (III) is oxidized by carbonate to Ce (IV), which is then preferentially adsorbed, leading to the development of negative Ce anomaly in the fluids (Pourret et al., 2008). The negative Ce anomaly in the hydrothermal dolomite was inherited from the host dolomite (Fig. 8). However, the degree of negative Ce anomalies in the three zones is different (Fig. 8), indicating that physiochemical conditions changed during the evolution of ore-forming fluids (Bau, 1991). Pourret et al. (2008) demonstrate that negative Ce anomalies are clearly developed in high pH environments. The strong negative Ce anomaly of dolomite in the ore indicated an alkaline environment. From the ore, transitional zone, to the wall rock, the Ce anomaly degree gradually weakens, which indicates that ore-forming fluids in the three-zone has evolved from alkaline to neutral and weakly acidic. These observations are consistent with the results of previous research that Pb-Zn ores are easiest to precipitate in an alkaline environment (Zhang, 2006; Zhang, 2016; Zhang et al., 2019).

6.2. *Sulfur and Pb isotope constraint on changes in fluids composition*

The in-situ $\delta^{34}S$ values of the sphalerite in the ore are higher than that in the transitional zone, and the $\delta^{34}S$ values of sphalerite grains in the transitional zone gradually decrease from the core to the rim (the maximum difference is 4.1‰) (Fig. 9), which are possibly caused by:(1) kinetic Rayleigh fractionation, (2) progressive evolution of the ore-forming fluids, and (3) change in physiochemical conditions (Seal, 2006). When the mineralizing fluid mixes with the sulfate-rich fluids, thermochemical sulfate reduction (TSR) is initiated, resulting in the precipitation of a significant amount of sulfide minerals (Huang et al., 2004; Leach et al., 2005; Leach et al., 2010). The rapid precipitation of sulfide minerals can cause kinetic Rayleigh fractionation of S isotopes during fluids mixing (Zhou et al., 2018c; Zhang et al., 2022). As the fluids evolves from the ore, transitional zone, to the wall rock, the sphalerite of the ore zone preferentially precipitates and tends to exhibit an enrich heavy sulfur isotope (^{34}S). The relative concentration of ^{32}S in fluids increases during the process of fluids evolution, causing a continuous increase in $\delta^{32}S$ values of later-precipitated sulfide minerals (the sphalerite in the transitional zone) (Zhang et al., 2022). Moreover, the factors influencing S isotopes change are temperature, pH, and fO_2 (O'Neil, 1986). The homogenization temperature of fluids inclusions in the sphalerite varies from 131 to 280 °C (Zhang et al., 2017). However, the S isotopic fractionation between H_2S and ZnS is very small (less than1.0‰) within this temperature range (Ohmoto, 1972). In addition, Ohmoto (1972) calculated that changes in pH and fO_2 within the stability field of sphalerite would have an insignificant influence on the $\delta^{34}S$ variation (~0.5‰). Consequently, the kinetic Rayleigh fractionation and progressive evolution of the ore-forming fluids explain the lower $\delta^{34}S$ of the sphalerite in the transitional zone, and the decreasing $\delta^{34}S$ of sphalerite grains from the core to the rim, although the influence of temperature, pH, and/or fO_2 cannot be entirely ruled out.

The different REE patterns between hydrothermal dolomite and unmineralized dolomite suggest that fluid-rock ratios during mineralization were high and the hydrothermal dolomite inherits the characteristics of ore-forming fluids (Qing and Mountjoy, 1994). The Pb isotopic composition of dolomite in the three zones is much lower than that of dolomite in the strata, which also shows that dolomite in the three zones inherits the lower Pb isotopic composition of the ore-forming fluids. However, the enhancement of the fluid-rock interaction accelerated the absorption of wall rock materials (Zhu et al., 2022). As the fluids evolves from the ore to the wall rock, the increased Pb isotopic compositions of galena from the ore, transitional zone, to the

Table 5
In situ Pb isotopic composition of galena from the Huize Pb-Zn deposit.

NO.	Sample Location	Experimental location	$^{206}Pb/^{204}Pb$	±2σ	$^{207}Pb/^{204}Pb$	±2σ	$^{208}Pb/^{204}Pb$	±2σ
KB-2-1	1237 *m*	Ore	18.482	0.003	15.720	0.003	38.909	0.010
KB-2-2		Ore	18.481	0.003	15.721	0.003	38.910	0.009
KB-2-3		Ore	18.484	0.003	15.721	0.003	38.911	0.008
KB-2-4		Transitional zone	18.489	0.002	15.737	0.002	38.956	0.006
KB-2-5		Ore	18.477	0.003	15.721	0.003	38.911	0.009
KB-2-6		ore	18.480	0.004	15.715	0.004	38.895	0.011
KB-2-7		Transitional zone	18.487	0.003	15.735	0.002	38.944	0.020
KB-2-8		Ore	18.474	0.005	15.715	0.004	38.889	0.012
KB-2-9		Transitional zone	18.487	0.003	15.737	0.002	38.963	0.005
KB-2-10		Ore	18.475	0.003	15.722	0.003	38.899	0.007
KB-2-11		Ore	18.481	0.002	15.722	0.002	38.914	0.005
KB-3-01	1199 *m*	Wall rock	18.502	0.002	15.741	0.002	38.995	0.008
KB-3-02		Wall rock	18.505	0.002	15.744	0.001	39.003	0.006
KB-3-03		Transitional zone	18.496	0.003	15.730	0.003	38.938	0.019
KB-3-04		Transitional zone	18.502	0.002	15.737	0.002	38.982	0.008
KB-3-05		Wall rock	18.502	0.002	15.741	0.002	38.995	0.011
KB-3-06		Wall rock	18.503	0.002	15.742	0.002	38.986	0.016
KB-3-07		Wall rock	18.497	0.003	15.743	0.002	38.994	0.007
KB-3-08		Transitional zone	18.499	0.002	15.739	0.002	38.982	0.007

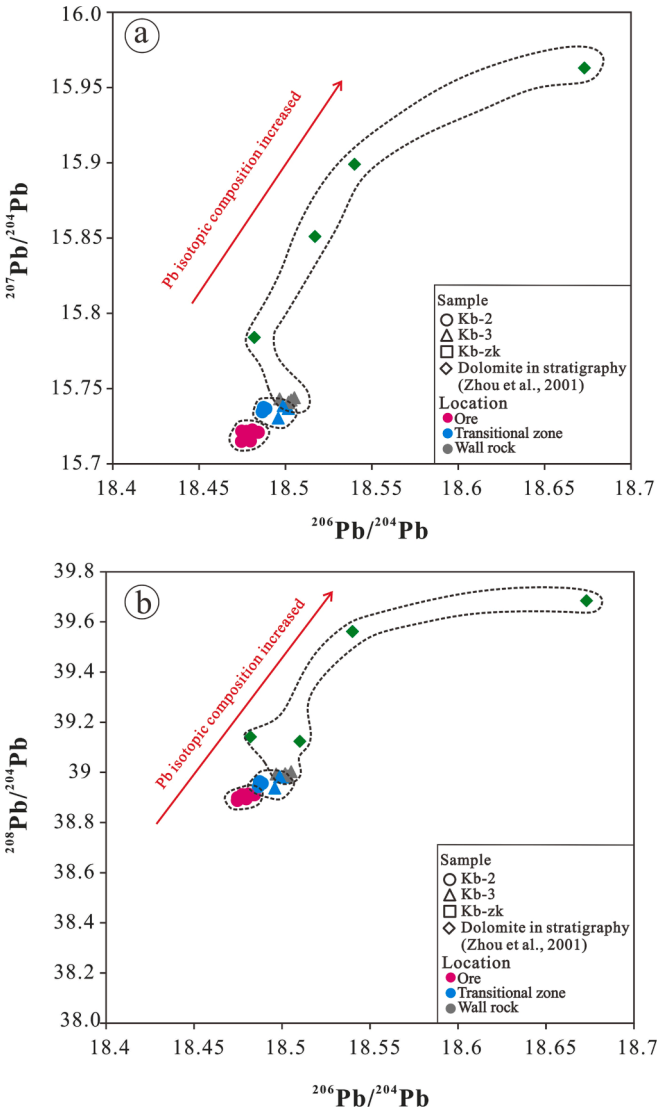

Fig. 10. Plots of $^{207}Pb/^{204}Pb$ vs. $^{206}Pb/^{204}Pb$(a) and $^{208}Pb/^{204}Pb$ vs. $^{206}Pb/^{204}Pb$(b) that show the variation in Pb isotopic composition of galena from ore, transitional zone, to wall rock, and lead isotope composition of wall-rock dolomite is from Zhou et al. (2001).

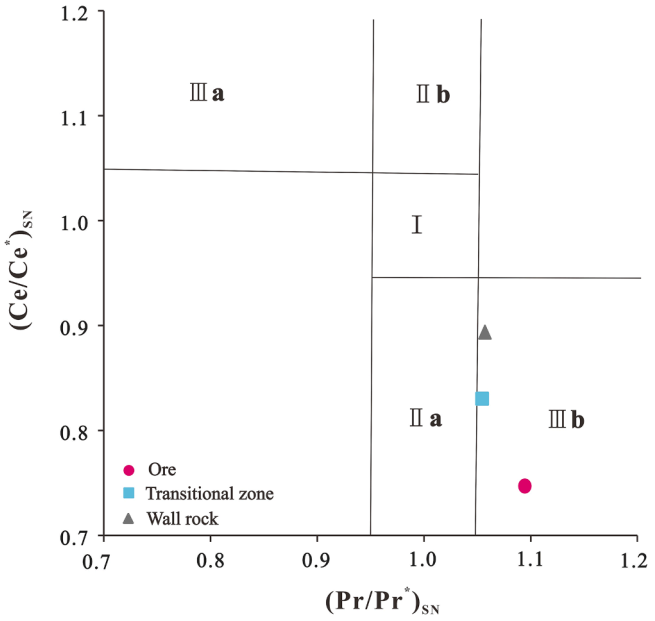

Fig. 11. The dolomite in different zones of Huize Pb-Zn deposit in a graph of $(Ce/Ce^*)_{SN}$ VS $(Pr/Pr^*)_{SN}$. Field I: neither Ce_{SN} nor La_{SN} anomaly; field IIa: positive La_{SN} anomaly, no Ce_{SN} anomaly; field IIb: negative Lass anomaly, no Ce_{SN} anomaly; field IIIa: positive Ce_{SN} anomaly; field IIIb: negative Ce_{SN} anomaly (modified after Bau and Dulski, 1996). The Ce/Ce* and Eu/Eu* values were calculated geometrically (cf., Bau and Dulski, 1996), $(Ce/Ce^*)_{SN} = Ce_{SN} / (0.5La_{SN} + 0.5Pr_{SN})$; $(Pr/Pr^*)_{SN} = Pr_{SN}/ (0.5Ce_{SN} + 0.5Nd_{SN})$ (The average content used in the calculation).

wall rock (Fig. 10) indicate increased involvement of dolostone with proceeding fluid-rock interaction. Therefore, Pb isotopic variation can be used as an important indicator for fluid-rock interaction.

6.3. *Ore-forming process*

Previous investigations have commonly believed that the Huize Pb-Zn deposit is the result of the mixing of multiple sources (Huang et al., 2004; Han et al., 2007; Li et al., 2006, 2007; Zhang et al., 2016; Zhang et al., 2017). The ore-forming fluids migrate from the deep basement of the Kunyang Group to shallow sections, flowing through host Lower Cambrian to Middle Permian carbonate rocks. The intense mineralization occurs between ore-forming fluids and carbonate rocks during their

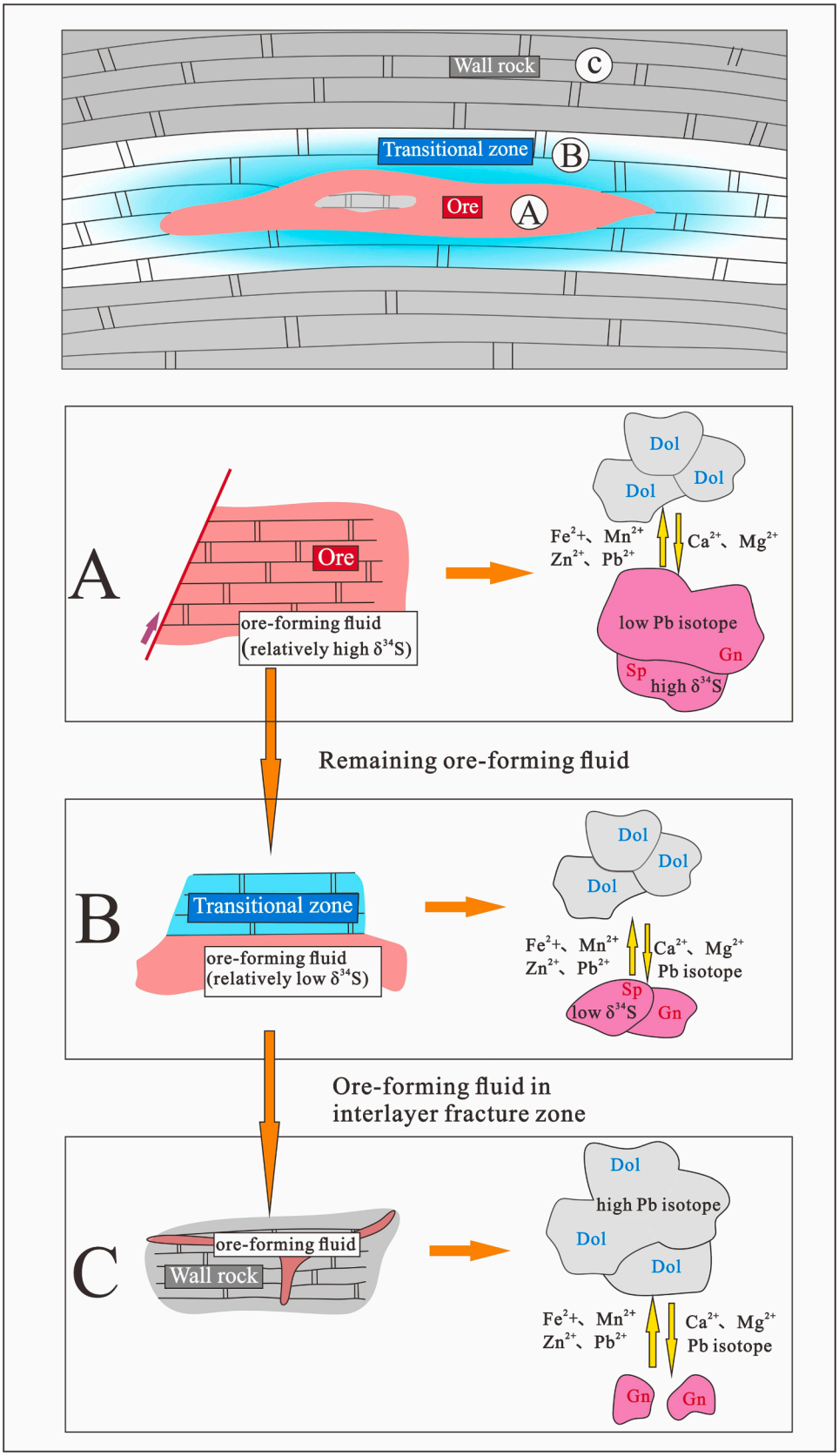

Fig. 12. Schematic diagram of ore-forming process from Huize Pb-Zn deposit. (a) In the ore body, the interaction between ore-forming fluids with relatively high $\delta^{34}S$ values and low Pb isotope combinations and the dolomite in the stratigraphy with high Ca^{2+}, Mg^{2+} and Pb isotopes, exchange of trace elements and isotopes; (b)In the contact zone, remaining ore-forming fluids with relatively low $\delta^{34}S$ values continue to interact with dolostone in the stratigraphy, trace elements and isotopes continue to exchange ; (c) In the wall rock, the interaction between the ore-forming fluids in the interlayer fracture zone and stratigraphic dolomite with higher Pb isotopic compositions, trace elements and isotopes continue to exchange. Gn: galena; Sp: sphalerite; Py: pyrite; Dol: dolomite.

ascending from the depth, resulting in isotope exchange. Such that the final composition of the S, Pb, Sr, Zn, Cd, C–O, and H–O isotopes of mixed fluids was in between that of deep ore-forming fluids and carbonate rocks (Li et al., 2006; Bao et al., 2017; Oyebamiji et al., 2020; Zhu et al., 2021; Zhang et al., 2022). These studies provide constraints on the ore-forming process from a macro scale. Therefore, our study from the thin section scale provides a more detailed view for the ore-forming process.

By summarizing in situ elemental and isotopic results, we propose a detailed model for the ore-forming process (Fig. 12). The dolomite in the stratigraphy is characterized by high Ca^{2+}, Mg^{2+}, and Pb isotopic ratios (Zhou et al., 2001). When deep ore-forming fluids enters the dolostone along fractures and interlayer fracture zone, where slight fluctuations in the physicochemical conditions of the fluids occur and the sulfide minerals precipitate, resulting in elements and isotopes exchange. The deep ore-forming fluids with higher $\delta^{34}S$ values and lower Pb isotope compositions preferentially precipitated as sphalerite and galena within the ore. The ore-forming fluids constantly exchange elements with dolomite during alteration and mineralization. The Mn, Fe, In, and V elements readily substitute Ca^{2+} and Mg^{2+} in dolomite, which may be consumed due to partition into the dolomite. The intense mineralization is favorable for the incorporation of ore elements such as Cu, Zn, Ag, and Cd into the dolomite, resulting in the dolomite in the ore enriched in these elements. As the fluids evolves towards the wall rock, the relative concentration of ^{32}S in fluids increases, leading to lower $\delta^{34}S$ values within the sphalerite in the transitional zone. At the same time, the mineralization weakens and the remaining fluids contains low content of ore-forming elements, resulting in reduced contents of Mn, Fe, In, V elements within the dolomite of the transitional zone and wall rock. Finally, the ore-forming fluids in the interlayer fracture zone continuously extract high Pb isotopic compositions from dolomite in the wall rocks, so the Pb isotopic compositions of galena in ore → transitional zone → wall rock are constantly increasing.

During the ore-forming process, the role of carbonate wall rock is crucial. The dolomite in the dolostone undergoes repeated dissolution–recrystallization (Fig. 5d, e), potentially acting as a buffer for the ore-forming fluids (Warren, 2000). In addition, the carbonate rocks with good permeability have given impetus to the migration and precipitation of the hydrothermal fluids (Huang et al., 2019). The continuous dissolution of dolostone produces a large amount of CO_2 to adjust the physicochemical conditions (such as pH, Eh) in the ore-forming fluids. The dolostone buffers acidity and alkalinity and promotes sulfide minerals precipitation (Liu et al., 2021). The reaction process is as follows:

$$ZnCl_4^{2-} + H_2S = ZnS_{(sphalerite)} + 4Cl^- + 2H^+ \quad (1)$$

$$PbCl_3^- + H_2S = PbS_{(galena)} + 3Cl^- + 2H^+ \quad (2)$$

$$CaMg(CO_3)_{2(dolostone)} + H^+ = Ca^{2+} + Mg^{2+} + CO_2\uparrow + H_2O \quad (3)$$

In summary, carbonate rocks are involved in sulfide mineralization through water–rock interaction (Zhou et al., 2022). The ore-forming fluids interacted with the dolomitic wall rock and an exchange of elements and isotopes between fluids and dolostone occur. As the relative evolution direction of ore-forming fluids from the ore, transitional zone, to the wall rock, the fluids pH evolves from alkaline to neutral and weakly acidic. In the ore-forming process, carbonate continuously consumes the acid due to the fluid-rock interaction, causing the pH to rise and the ore-forming elements precipitate to form sphalerite with a relatively low $\delta^{34}S$ value and galena with high Pb isotopic composition. Therefore, pH change induced by carbonate dissolution during the ore-forming process is likely critical in ore deposition.

7. Conclusion

1. Systematic variations in the occurrences of dolomite are identified from replacement to veins in the ore, transitional zone, and wall rock.
2. From the ore, transitional zone, to the wall rock, increased Ca, Mg, and REE in dolomite and decreased Mn, Fe, In, and V, weakened negative Ce anomaly and constant negative Eu anomaly, indicate that fluids changes from alkaline to neutral and weakly acidic under relatively low temperature during intensive fluid-rock interaction.
3. The decreased $\delta^{34}S$ value of sphalerite from the ore to the transitional zone and from the core to the rim for a single grain, which can be interpreted as kinetic fractionation of sulfur isotopes induced by the precipitation of sulfides. The increased Pb isotopic composition of the galena from the ore, transitional zone, to the wall rock, indicates increased involvement of the dolostone.
4. A new model for the ore-forming process is proposed. Ore-forming fluids (rich in ore elements, with higher $\delta^{34}S$ value and low Pb isotope compositions) enter the dolostone (high Pb isotope compositions), leading to intense fluid-rock interaction and extensive exchange of elements and isotopes between fluids and dolostone. Carbonate continuously consumes the acid due to the mineralization, causing the pH to rise and the ore-forming elements precipitate as sphalerite and galena. The pH change is possibly the significant factor for sulfide precipitation.

Declaration of Competing Interest

The authors declare that they have no known competing financial interests or personal relationships that could have appeared to influence the work reported in this paper.

Data availability

No data was used for the research described in the article.

Acknowledgments

This research was financially supported by the National Natural Science Foundation of China (92162218 and 42202099), the CAS Hundred Talents Program to XWH, Guizhou Provincial 2021 Science and Technology Subsidies (GZ2021SIG)and Major Collaborative Innovation Projects for Prospecting Breakthrough Strategic Action of Guizhou Province, China ([2022] ZD004).

References

Anderson, G.M., 1983. Some geochemical aspects of sulfide precipitation in carbonate rocks. In: Kisvarsanyi, G., Grant, S.K., Pratt, W.P., Keonig, J.W. (Eds.), International Conference on Mississippi Valley Type Lead-Zinc Deposits, Proceedings. Missouri, Rolla, pp. 61–76.

Anderson, G.M., Macqueen, R.W., 1982. Ore deposit models-6. Mississippi Valley-type lead-zinc deposits. Geosci. Can. 9, 108–117.

Banner, J.L., Hanson, G.N., Meyeks, W.J., 1988b. Fluid-rock interaction history of regionally extensive dolomites of the Burlington-Keokuk Formation (Mississippian): isotope evidence. In: Sedimentohgy und Geochemistrj) of Dolostones (Ed. V. Shukla & P.A. Baker), Spec. Publ. Soc. econ. Palront. Miner. 43, 97–113.

Banner, J.L., Hanson, G.N., Meyeks, W.J., 1988. Rare earth element and Nd isotopic variations in regionally extensive dolomites from the Burlington-Keokuk Formation (Mississippian): implications for REE mobility during carbonate diagenesis. J. Sedim. Prtrol. 58, 415–432.

Bao, Z.A., Yuan, W.T., Yuan, H.L., Liu, X., Chen, K.Y., Zong, C.L., 2016. Non-matrix-matched determination of lead isotope ratios in ancient bronze artifacts by femtosecond laser ablation multi-collector inductively coupled plasma mass spectrometry. Int. J. Mass Spectrom. 402, 12–19.

Bao, Z.A., Chen, L., Zong, C.L., Yuan, H.L., Chen, K.Y., Dai, M.L., 2017. Development of pressed sulfide powder tablets for in-situ sulfur and lead isotope measurement using LA-MC-ICP-MS. Int. J. Mass Spectrom. 421, 255–262.

Bau, M., 1991. Rare-earth element mobility during hydrothermal and metamorphic fluid–rock interaction and the significance of the oxidation state of europium. Chem. Geol. 93 (3-4), 219–230.

Bau, M., Dulski, P., 1996. Distributions of yttrium and rare-earth elements in the Penge and Kuruman iron-formation, Transvaal Supergroup, South Africa. Precambr. Res. 79 (1–2), 37–55.
Bau, M., Moller, P., 1992. Rare earth element fractionation in metamorphogenic hydrothermal calcite, magnesite and sideriteFraktionierung der seltenen Erd-Elemente in metamorphogenen hydrothermoclen Calciten, Magnesiten und Sideriten. Mineral. Petrol. 45 (3-4), 231–246.
Bau, M., Romer, R.L., Lüders, V., Dulski, P., 2003. Tracing element sources of hydrothermal mineral deposits: REE and Y distribution and Sr-Nd-Pb isotopes in fluorite from MVT deposits in the Pennine Orefield, England. Miner. Deposita 38 (8), 992–1008.
Bolhar, R., Van Kranendonk, M.J., 2007. A non-marine depositional setting for the northern Fortescue Group, Pilbara Craton, inferred from trace element geochemistry of stromatolitic carbonates. Precambr. Res. 155 (3–4), 229–250.
Chen, L., Liu, Y.S., Hu, Z.C., Gao, S., Zong, K.Q., Chen, H.H., 2011. Accurate determinations of fifty-four major and trace elements in carbonate by LA-ICP-MS using normalization strategy of bulk components as 100%. Chem. Geol. 284 (3–4), 283–295.
Chen, L., Yuan, H.L., Chen, K.Y., Bao, Z.A., Zhu, L.M., Liang, P., 2019. In situ sulfur isotope analysis by laser ablation MC-ICPMS and a case study of the Erlihe Zn-Pb ore deposit, Qinling orogenic belt, Central China. J. Asian Earth Sci. 176, 325–336.
Chen, Y.Q., Zhou, X.Y., Jiang, S.Y., Zhao, K.D., 2013. Types and origin of dolostones in Tarim Basin, Northwest China: petrographic and geochemical evidence. Acta Geol. Sin. – Engl. 87 (2), 467–485.
Craddock, P.R., Bach, W., Seewald, J.S., Rouxel, O.J., Reeves, E., Tivey, M.K., 2010. Rare earth element abundances in hydrothermal fluids from the Manus Basin, Papua New Guinea: Indicators of sub-seafloor hydrothermal processes in back-arc basins. Geochim. Cosmochim. Acta 74 (19), 5494–5513.
Debruyne, D., Hulsbosch, N., Muchez, P., 2016. Unraveling rare earth element signatures in hydrothermal carbonate minerals using a source-sink system. Ore Geol. Rev. 72, 232–252.
Frondini, F., Zucchini, A., Comodi, P., 2014. Water-rock interactions and trace elements distribution in dolomite aquifers: The Sassolungo and Sella systems (Northern Italy). Geochem. J. 48 (3), 231–246.
Han, R.S., Liu, C.Q., Huang, Z.L., Ma, D.Y., Li, Y., Hu, B., Ma, G.S., Lei, L., 2004. Fluid inclusion of calcite and sources of ore-forming fluids in the Huize Zn-Pb-(Ag-Ge) district, Yunnan, China. Acta Geol. Sin. (Engl. Ed.) 78, 583–591.
Han, R.S., Hu, Y.Z., Wang, X.K., Huang, Z.L., Chen, J., Wang, F., Wu, P., Li, B., Wang, H. J., Dong, Y., Lei, L., 2012. Mineralization model of rich Ge-Ag-bearing Pb-Zn polymetallic deposit concentrated district in northeastern Yunnan, China. Acta Geol. Sin. 86, 280–294 in Chinese with English abstract.
Han, R.-S., Liu, C.-Q., Huang, Z.-L., Chen, J., Ma, D.-Y., Lei, L.i., Ma, G.-S., 2007. Geological features and origin of the Huize carbonate-hosted Zn-Pb-(Ag) district, Yunnan, South China. Ore Geol. Rev. 31 (1-4), 360–383.
Han, R.S., Wang, F., Hu, Y.Z., Wang, X.K., Ren, T., Qiu, W.L., Zhong, K.H., 2014. Metallogenic tectonic dynamics and chronology constrains on the Huize-type (HZT) Germanium-Rich Silver-Zinc-Lead Deposits. Geotect. Metal. 38, 758–771 in Chinese with English abstract.
Hecht, L., Freiberger, R., Gilg, H.A., Grundmann, G., Kostitsyn, Y.A., 1999. Rare earth element and isotope (C, O, Sr) characteristics of hydrothermal carbonates: genetic implications for dolomite-hosted talc mineralization at Göpfersgrün (Fichtelgebirge, Germany). Chem. Geol. 155 (1-2), 115–130.
Hu, R.Z., Fu, S.L., Huang, Y., Zhou, M.F., Fu, S.H., Zhao, C.H., Wang, Y.J., Bi, X.W., Xiao, J.F., 2017. The giant South China Mesozoic low-temperature metallogenic domain: Reviews and a new geodynamic model. J. Asian Earth Sci. 137, 9–34.
Hu, R.-Z., Zhou, M.-F., 2012. Multiple Mesozoic mineralization events in South China—an introduction to the thematic issue. Miner. Deposita 47 (6), 579–588.
Huang, Z.L., Chen, J., Han, R.S., Li, W.B., Liu, C.Q., Zhang, Z.L., Ma, D.Y., Gao, D.R., Yang, H.L., 2004. Geochemistry and ore-formation of the Huize giant lead–zinc deposit, Yunnan, Province, China. Discussion on the relationship between Emeishan flood basalts and lead–zinc mineralization. Geological Publishing House, Beijing, pp. 1–204 (in Chinese).
Huang, Z.L., Li, X.B., Zhou, M.F., Li, W.B., Jin, Z.G., 2010. REE and C-O isotopic geochemistry of calcites from the world-class Huize Pb–Zn deposit, Yunnan, China: implications for the ore genesis. Acta Geol. Sin. (Engl. Ed.) 84, 597–613.
Huang, C.W., Li, H., Lai, C.K., 2019. Genesis of the Binh Do Pb-Zn deposit in northern Vietnam: Evidence from H-O-S-Pb isotope geochemistry. J. Earth Sci. 30 (4), 679–688.
Jochum, K.P., Scholz, D., Stoll, B., Weis, U., Wilson, S.A., Yang, Q.C., Schwalb, A., Börner, N., Jacob, D.E., Andreae, M.O., 2012. Accurate trace element analysis of speleothems and biogenic calcium carbonates by LA-ICP-MS. Chem. Geol. 318–319, 31–44.
Komiya, T., Hirata, T., Kitajima, K., Yamamoto, S., Shibuya, T., Sawaki, Y., Ishikawa, T., Shu, D., Li, Y., Han, J., 2008. Evolution of the composition of seawater through geologic time, and its influence on the evolution of life. Gondwana Res. 14 (1-2), 159–174.
Leach, D.L., Sangster, D.F., Kelley, K.D., Large, R.R., Garven, G., Allen, C.R., Gutzmer, J., Walters, S.G., 2005. Sediment-hosted Lead-Zinc deposits: a global perspective. Econ. Geol. 100th Anniversary, 561–608.
Leach, D.L., Bradley, D.C., Huston, D., Pisarevsky, S.A., Taylor, R.D., Gardoll, S.J., 2010. Sediment-hosted lead–zinc deposits in Earth history. Econ. Geol. 105 (3), 593–625.
Li, Z.T., Han, R.S., Yan, Q.W., 2017. Mineralization-alteration zoning regularity and structural ore-controlling role in the Huize super-large sized Ge-Ag-rich Pb-Zn deposit, Yunnan Province. Geol. China 44, 316–330 in Chinese with English abstract.
Li, W.B., Huang, Z.L., Zhang, G., 2006. Sources of the ore metals of the Huize ore field in Yunnan province: constraints from Pb, S, C, H, O and Sr isotope geochemistry. Acta Petrol. Sin. 22 (10), 2567–2580.
Li, W., Huang, Z., Yin, M., 2007. Dating of the giant Huize Zn–Pb ore field of Yunnan province, southwest China: constraints from the Sm–Nd system in hydrothermal calcite. Resour. Geol. 57 (1), 90–97.
Li, W.B., Huang, Z.L, Yin, M.D., 2007. Isotope geochemistry of the Huize Zn–Pb ore field, Yunnan province, southwestern China: implication for the sources of ore fluid and metals. Geochem. J. 41 (1), 65–81.
Liu, H.C., Lin, W.D., 1999. Study on the law of Pb–Zn–Ag ore deposit in northeast Yunnan, China. Yunnan University Press, Kunming, pp. 1–468 in Chinese.
Liu, W.H., Spinks, S.C., Glenn, M., MacRae, C., Pearce, M.A., 2021. How carbonate dissolution facilitates sediment-hosted Zn-Pb mineralization. Geology 49 (11), 1363–1368.
Lüders, V., Möller, P., Dulski, P., 1993. REE fractionation in carbonates and fluorites. In: Moeller, P., Lüders, V. (Eds.), Formation of hydrothermal vein deposits monograph series on mineral Deposits. Gebrüter Borntraeger, Berlin, pp. 133–150.
Luo, K., Zhou, J.X., Huang, Z.L., Caulfield, J., Zhao, J.X., Feng, Y.X., Ouyang, H.G., 2019. New insights into the evolution of MVT hydrothermal system: A case study of the Wusihe Pb-Zn deposit (South China), using quartz in situ trace elements and sulfides in situ S-Pb isotopes. Am Mineral. 105, 31–51.
Luo, K., Zhou, J.X., Huang, Z.L., Wang, X.C., Wilde, S.A., Zhou, W., Tian, L., 2019. New insights into the origin of Early Cambrian carbonate-hosted Pb-Zn deposits in South China: A case study of the Maliping Pb-Zn deposit. Gondwana Res. 70, 88–103.
Magnall, J.M., Gleeson, S.A., Blamey, N.J.F., Paradis, S., Luo, Y., 2016. The thermal and chemical evolution of hydrothermal vent fluids in shale hosted massive sulphide (SHMS) systems from the MacMillan Pass district (Yukon, Canada). Geochim. Cosmochim. Acta 193, 251–273.
Meng, Y.-M., Hu, R.-Z., Huang, X.-W., Gao, J.-F., Sasseville, C., 2019. The origin of the carbonate-hosted Huize Zn–Pb–Ag deposit, Yunnan province, SW China: constraints from the trace element and sulfur isotopic compositions of pyrite. Mineral. Petrol. 113 (3), 369–391.
Migdisov, A.A., Williams-Jones, A.E., Wagner, T., 2009. An experimental study of the solubility and speciation of the Rare Earth Elements (III) in fluoride-and chloride-bearing aqueous solutions at temperatures up to 300°C. Geochim. Cosmochim. Acta 73 (23), 7087–7109.
Millet, M.A., Baker, J.A., Payne, C.E., 2012. Ultra-precise stable Fe isotope measurements by high resolution multiple-collector inductively coupled plasma mass spectrometry with a ^{57}Fe–^{58}Fe double spike. Chem. Geol. 304–305, 18–25.
Nagender Nath, B., Bau, M., Ramalingeswara Rao, B., Rao, C.M., 1997. Trace and rare earth elemental variation in Arabian Sea sediments through a transect across the oxygen minimum zone. Geochim. Cosmochim. Acta 61 (12), 2375–2388.
O'Neil, J.R., 1986. Theoretical and experimental aspects of isotopic fractionation. Rev Mineral. 16, 1–40.
Ohmoto, H., 1972. Systematics of sulfur and carbon isotopes in hydrothermal ore deposits. Econ. Geol. 67, 551–578.
Oyebamiji, A., Hu, R., Zhao, C., Zafar, T., 2020. Origin of the Triassic Qilinchang Pb-Zn deposit in the western Yangtze block, SW China: Insights from in-situ trace elemental compositions of base metal sulphides. J. Asian Earth Sci. 192, 104292.
Oyebamiji, A., Hu, R.Z., Zhao, C.H., Zhaanbaeva, A., Zafar, T., 2020. Ore genesis of the Qilinchang Carboniferous carbonate Pb-Zn Mississippi Valley-type deposit, Western Yangtze Platform, southwest China: Constraints from mineralogy, C-O-S-Pb isotope systematics, and REE studies. Episodes. J. Inter. Geosci. 43 (2), 761–784.
Oyebamiji, A., Falae, P., Zafar, T., Rehman, H.U., Oguntuase, M., 2023. Genesis of the Qilinchang Pb–Zn deposit, southwestern China: Evidence from mineralogy, trace elements systematics and S-Pb isotopic characteristics of sphalerite. Appl. Geochem. 148, 105545.
Perry, E.P., Gysi, A.P., 2018. Rare earth elements in mineral deposits: speciation in hydrothermal fluids and partitioning in calcite. Geofluids 2018, 1–19.
Pourret, O., Davranche, M., Gruau, G., Dia, A., 2008. New insights into cerium anomalies in organic-rich alkaline waters. Chem. Geol. 251 (1–4), 120–127.
Qing, H., Mountjoy, E.W., 1994. Rare earth element geochemistry of dolomites in the Middle Devonian Presqu'ile barrier, Western Canada Sedimentary Basin: implications for fluid-rock ratios during dolomitization. Sedimentology 41 (4), 787–804.
Qiu, Y.M., Gao, S., McNaughton, N.J., Groves, D.I., Ling, W.L., 2000. First evidence of N3.2 Ga continental crust in the Yangtze craton of south China and its implications for Archean crustal evolution and Phanerozoic tectonics. Geology 28, 11–14.
Rieger, P., Magnall, J.M., Gleeson, S.A., Oelze, M., Wilke, F.D.H., Lilly, R., 2022. Differentiating between hydrothermal and diagenetic carbonate using rare earth element and yttrium (REE+Y) geochemistry: a case study from the Paleoproterozoic George Fisher massive sulfide Zn deposit, Mount Isa, Australia. Miner. Deposita 57 (2), 187–206.
Rimstidt, J.D., Balog, A., Webb, J., 1998. Distribution of trace elements between carbonate minerals and aqueous solutions. Geochim. Cosmochim. Acta 62 (11), 1851–1863.
Seal, R.R., 2006. Sulfur Isotope Geochemistry of Sulfide Minerals. Rev. Mineral. Geochem. 61 (1), 633–677.
Shannon, R.D., 1976. Revised effective ionic radii and systematic studies of interatomic distances in halides and chalcogenides. Acta Crystallogr. Sect. A 32 (5), 751–767.
Tan, M., Wu, P., Han, R.S., Zhang, Y., Huang, Z.L., Jiang, L.Y., Yang, H., 2022. Genesis of coarse-giant carbonate rocks in Maoping and Huize super-large lead—zinc deposits in Northeast Yunnan and its prospecting significance. Geol. Rev. 68 (01), 147–166 in Chinese with English abstract.
Tan, M., Wu, P., Han, R.S., Zhang, Y., Huang, Z.L., Yang, H., 2022. Geochemical characteristics of in-situ micro-analyzed dolomites in "ore-contact zone-wall rock" of

the Huize super-large lead-zinc deposit and their indicative significances. Acta Mineral. Sin. 42 (03), 315–328 in Chinese with English abstract.
Tan, S.C., Zhou, J.X., Li, B., Zhao, J.X., 2017. In situ Pb and bulk Sr isotope analysis of the Yinchanggou Pb-Zn deposit in Sichuan Province (SW China): Constraints on the origin and evolution of hydrothermal fluids. Ore Geol. Rev. 91, 432–443.
Tang, Y.Y., Bi, X.W., Zhou, J.X., Liang, F., Qi, Y.Q., Leng, C.B., Zhang, H., 2019. Rb-Sr isotopic age, S-Pb-Sr isotopic compositions and genesis of the ca. 200Ma Yunluheba Pb-Zn deposit in NW Guizhou Province, SW China. J. Asian Earth Sci. 185, 104054.
Taylor, S.R., Mclennan, S.M., 1985. The continental crust: Its composition and evolution, an examination of the geochemical record preserved in sedimentary rocks. Blackwell Scientific Pub, Oxford, pp. 1–328.
Wang, L.J., Mi, M., Zhou, J.X., Luo, K., 2018. New constraints on the origin of the Maozu carbonate-hosted epigenetic Zn-Pb deposit in NE Yunnan Province, SW China. Ore Geol. Rev. 101, 578–594.
Warren, J., 2000. Dolomite: Occurrence, evolution and economically important associations. Earth-Sci. Rev. 52 (1–3), 1–81.
Wen, D.X., Han, R.S., Wu, P., He, J.J., 2014. Altered dolomite features and petro-geochemical prospecting indicators in the Huize lead-zinc deposit. Geol. China 41, 235–245 in Chinese with English abstract.
Williams-Jones, A.E., Migdisov, A.A., Samson, I.M., 2012. Hydrothermal mobilisation of the rare earth elements–a tale of "ceria" and "yttria". Elements 8 (5), 355–360.
Wogelius, R.A., Fraser, D.G., Feltham, D.J., Whiteman, M.I., 1992. Trace element zoning in dolomite: proton microprobe data and thermodynamic constraints on fluid compositions. Geochim. Cosmochim. Acta 56 (1), 319–334.
Wu, Y., 2013. The Age and Ore-Forming Process of MVT Deposits in the Boundary Area of Sichuan-Yunnan-Guizhou Provinces, Southwest China. Ph.D. Thesis, China University of Geosciences, Beijing, China, pp. 1–167 (In Chinese).
Xu, C., Zhong, H., Hu, R.Z., Wen, H.J., Zhu, W.G., Bai, Z.J., Fan, H.F., Li, F.F., Zhou, T., 2020. Sources and ore-forming fluid pathways of carbonate-hosted Pb-Zn deposits in Southwest China: implications of Pb-Zn-S-Cd isotopic compositions. Miner. Deposita 55 (3), 491–513.
Yan, D.-P., Zhou, M.-F., Song, H.-L., Wang, X.-W., Malpas, J., 2003. Origin and tectonic significance of a Mesozoic multi-layer over-thrust system within the Yangtze Block (South China). Tectonophysics 361 (3-4), 239–254.
Ye, L., Cook, N.J., Ciobanu, C.L., Yuping, L., Qian, Z., Tiegeng, L., Wei, G., Yulong, Y., Danyushevskiy, L., 2011. Trace and minor elements in sphalerite from base metal deposits in South China: a LA-ICPMS study. Ore Geol. Rev. 39 (4), 188–217.
Ye, L., Gao, W., Yang, Y., Tiegeng, L., Peng, S., 2012. Trace elements in sphalerite in Laochang Pb-Zn polymetallic deposit, Lancang, Yunnan Province. Acta Petrol. Sin. 28 (05), 1362–1372 in Chinese with English abstract.
Ye, L., Li, Z.L., Hu, Y.S., Huang, Z.L., Zhou, J.X., Fan, H.F., Danyushevskiy, L., 2016. Trace elements in sulfide from the Tianbaoshan Pb-Zn deposit, Sichuan Province, China: A LA-ICPMS study. Acta Petrol Sin. 32 (11), 3377–3393 in Chinese with English abstract.
Yuan, H.L., Yin, C., Liu, X., Chen, K.Y., Bao, Z.A, Zong, C.L., Dai, M.N., Lai, S.C., Wang, R., Jiang, S.Y., 2015. High precision in-situ Pb isotopic analysis of sulfide minerals by femtosecond laser ablation multi-collector inductively coupled plasma mass spectrometry. Sci. China. -Earth Sci. 58 (10), 1713–1721.
Zhang, Z.L., 2006. Feature and Sources of Ore-forming fluid in the Huize lead-zinc ore deposits, Yunnan province, China: Evidence from fluid inclusions and water-rock reaction experiments. In: The Institute of Geochemistry, Chinese Academy of Sciences, pp. 1–128.
Zhang, Y., 2016. Fluid mixing metallogenic mechanism of Huize super large Lead-Zinc Deposits in northeast of Yunnan poly-metallic mineralization domain. Kunming University of Science and Technology, Kunming, pp. 1–193.
Zhang, Y., Han, R., Wei, P., Qiu, W., 2017. Fluid inclusion features and physicochemical conditions of the Kuangshanchang Pb-Zn Deposit, Huize, Yunnan Province. J. Jilin Univ. 47, 719–733 in Chinese with English abstract.
Zhang, Y., Han, R.S., Ding, X., Wang, Y.R., Wei, P.T., 2019. Experimental study on fluid migration mechanism related to Pb–Zn super-enrichment: Implications for mineralization mechanisms of the Pb–Zn deposits in the Sichuan–Yunnan–Guizhou, SW China. Ore Geol. Rev. 114, 103110.
Zhang, Y., Runsheng, H., Lei, W., Wei, P., 2022. Zn–S isotopic fractionation effect during the evolution process of ore-forming fluids: A case study of the ultra-large Huize rich Ge-bearing Pb–Zn deposit. Appl. Geochem. 140, 105240.
Zhang, C.Q., Wu, Y., Hou, L., Mao, J.W., 2015. Geodynamic setting of mineralization of Mississippi Valley-type deposits in world-class Sichuan-Yunnan-Guizhou Zn-Pb triangle, Southwest China: Implications from age-dating studies in the past decade and the Sm-Nd age of Jinshachang deposit. J. Asian Earth Sci. 103, 103–114.
Zhong, S.J., Mucci, A., 1995. Partitioning of rare-earth elements (REE) between calcites and seawater solution at 25-degrees-C and 1atm, and high dissolved REE concentrations. Geochim. Cosmochim. Acta 59 (3), 443–453.
Zhou, J.X., Huang, Z.L., Bao, G.P., 2013b. Geological and sulfur–lead–strontium isotopic studies of the Shaojiwan Pb–Zn deposit, southwest China: implications for the origin of hydrothermal fluids. J. Geochem. Explor. 128, 51–61.
Zhou, J.X., Huang, Z.L., Gao, J.G., Yan, Z.F., 2013c. Geological and C-O–S–Pb–Sr isotopic constraints on the origin of the Qingshan carbonate-hosted Pb–Zn deposit, SW China. Int. Geol. Rev. 55, 904–916.
Zhou, J.X., Huang, Z.L., Yan, Z.F., 2013d. The origin of the Maozu carbonate-hosted Pb–Zn deposit, southwest China: constrained by C-O–S–Pb isotopic compositions and Sm–Nd isotopic age. J. Asian Earth Sci. 73, 39–47.
Zhou, J.X., Huang, Z.L., Zhou, M., Li, X., Jin, Z., 2013a. Constraints of C-O-S-Pb isotope compositions and Rb-Sr isotopic age on the origin of the Tianqiao carbonate-hosted Pb-Zn deposit, SW China. Ore Geol. Rev. 53, 77–92.
Zhou, J.X., Huang, Z.L., Zhou, M.F., Zhu, X.K., Muchez, P., 2014. Zinc, sulfur and lead isotopic variations in carbonate-hosted Pb–Zn sulfide deposits, southwest China. Ore Geol. Rev. 58, 41–54.
Zhou, J.X., Luo, K., Wang, X.C., Wilde, S.A., Wu, T., Huang, Z.L., Cui, Y.L., Zhao, J.X., 2018b. Ore genesis of the Fule Pb-Zn deposit and its relationship with the Emeishan Large Igneous Province: Evidence from mineralogy, bulk C-O-S and in situ S-Pb isotopes. Gondwana Res. 54, 161–179.
Zhou, J.X., Wang, X.C., Wilde, S.A., Luo, K., Huang, Z.L., Wu, T., Jin, Z.G., 2018c. New insights into the metallogeny of MVT Zn-Pb deposits: A case study from the Nayongzhi in South China, using field data, fluid compositions, and in situ S-Pb isotopes. Am. Mineral. 103, 91–108.
Zhou, C., Wei, C., Guo, J., Li, C., 2001. The source of metals in the Qilinchang Zn-Pb deposit, Northeastern Yunnan, China: Pb-Sr isotope constraints. Econ. Geol. 96 (3), 583–598.
Zhou, J.X., Xiang, Z.Z., Zhou, M.F., Feng, Y.X., Luo, K., Huang, Z.L., Wu, T., 2018a. The giant Upper Yangtze Pb-Zn province in SW China: Reviews, new advances and a new genetic model. J. Asian Earth Sci. 154, 280–315.
Zhou, J.-X., Yang, Z.-M., An, Y.-L., Luo, K., Liu, C., Ju, Y., 2022. An evolving MVT hydrothermal system: Insights from the Niujiaotang Cd-Zn ore field, SW China. J. Asian Earth Sci. 237, 105357.
Zhu, D.-P., Li, H., Jiang, W.-C., Wang, C., Hu, X.-J., Kong, H., 2022. Ore-forming environment of Pb-Zn mineralization related to granite porphyry at Huangshaping skarn deposit, Nanling Range, South China. T Nonferr Metal SOC. 32 (9), 3015–3035.
Zhu, C., Wen, H., Zhang, Y., Huang, Z., Cloquet, C., Luais, B., Yang, T., 2021. Cadmium isotopic constraints on metal sources in the Huize Zn–Pb deposit, SW China. Geosci. Front. 12 (6), 101241.